HHS Public Access

Author manuscript

Cell Rep. Author manuscript; available in PMC 2024 September 20.

Published in final edited form as:

Cell Rep. 2024 May 28; 43(5): 114169. doi:10.1016/j.celrep.2024.114169.

Smooth muscle cell-derived Cxcl12 directs macrophage accrual and sympathetic innervation to control thermogenic adipose tissue

Derek Lee[1,3], **Abigail M. Benvie**[1,3], **Benjamin M. Steiner**[1], **Nikolai J. Kolba**[1], **Josie G. Ford**[1], **Sean M. McCabe**[1], **Yuwei Jiang**[2], **Daniel C. Berry**[1,4,*]

[1]Division of Nutritional Sciences, Cornell University, Ithaca, NY 14853, USA

[2]Department of Physiology and Biophysics, University of Illinois at Chicago, Chicago, IL 60612, USA

[3]These authors contributed equally

[4]Lead contact

SUMMARY

Sympathetic innervation of brown adipose tissue (BAT) controls mammalian adaptative thermogenesis. However, the cellular and molecular underpinnings contributing to BAT innervation remain poorly defined. Here, we show that smooth muscle cells (SMCs) support BAT growth, lipid utilization, and thermogenic plasticity. Moreover, we find that BAT SMCs express and control the bioavailability of Cxcl12. SMC deletion of Cxcl12 fosters brown adipocyte lipid accumulation, reduces energy expenditure, and increases susceptibility to diet-induced metabolic dysfunction. Mechanistically, we find that Cxcl12 stimulates $CD301^{+}$ macrophage recruitment and supports sympathetic neuronal maintenance. Administering recombinant Cxcl12 to obese mice or leptin-deficient (Ob/Ob) mice is sufficient to boost macrophage presence and drive sympathetic innervation to restore BAT morphology and thermogenic responses. Altogether, our data reveal an SMC chemokine-dependent pathway linking immunological infiltration and sympathetic innervation as a rheostat for BAT maintenance and thermogenesis.

In brief

Lee et al. expose the role of $Cxcl12^{+}$ smooth muscle cells in coordinating brown adipose tissue (BAT) homeostasis. They find that Cxcl12 is necessary for BAT sympathetic innervation and macrophage accrual to stimulate thermogenesis, enhancing energy expenditure. Moreover, Cxcl12 administration alleviates obesogenic BAT dysfunction to restore thermogenesis.

*Correspondence: dcb37@cornell.edu.

AUTHOR CONTRIBUTIONS

Y.J. and D.C.B initiated the study. D.L., A.M.B., B.M.S., N.J.K., J.G.F., S.M.M., and D.C.B designed and performed the experiments, collected data, and analyzed the results. D.L., A.M.B., and D.C.B wrote the manuscript.

SUPPLEMENTAL INFORMATION

Supplemental information can be found online at https://doi.org/10.1016/j.celrep.2024.114169.

DECLARATION OF INTERESTS

The authors declare no competing interests.

Graphical Abstract

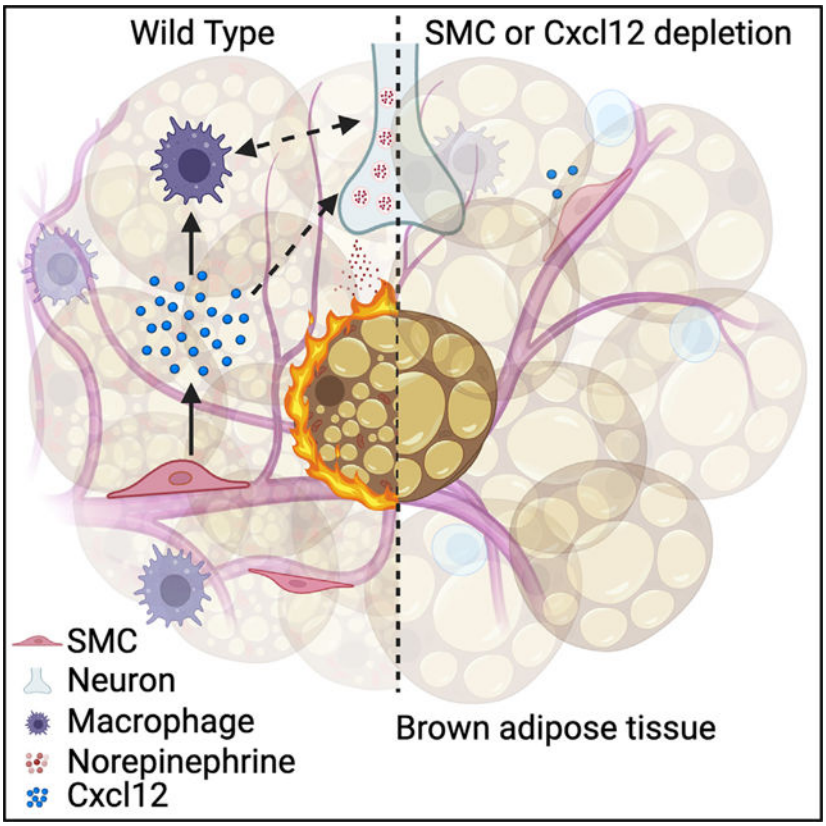

INTRODUCTION

Brown adipose tissue (BAT), a tissue specialized in non-shivering (adaptative) thermogenesis, has provided a significant evolutionary advantage for mammals to survive cold temperature exposure.[1] Brown adipocytes contain specialized mitochondria that express uncoupling protein 1 (Ucp1) to futilely burn glucose and free fatty acids to generate heat.[2] Because of this thermogenic ability, brown adipocytes have gained considerable clinical research attention as a potential cellular tool to counteract metabolic dysregulation in response to pathologic white adipose tissue (WAT) expansion.[3–5] However, BAT prevalence and induction in humans diminishes upon adult maturation and with aging.[6,7] The reasons for these vicissitudes are unclear; thus, identifying the cellular and molecular mechanisms controlling brown adipocyte thermogenic potential is critical for combating excess body fat.

To achieve thermogenesis, BAT is densely innervated with sympathetic neurons that release the neurotransmitter noradrenaline to stimulate fat cell lipolysis and energy uncoupling.[8,9] Therefore, the amount of BAT innervation is correlated with thermogenic capacity and macronutrient burning potential.[10] Correspondingly, blood vessels—often forming alongside nerve fibers—are critical for BAT oxygenation and nutrient supply and for carrying warmed blood to peripheral tissues.[11] In addition, parallels in growth factor signaling between axon and angiogenic sprouting have emerged as a cooperative system to direct innervation and

vascularization of target tissues.[12] Recently, adipocyte-expressing genes such as Prdm16 and S100B have been linked to the amount of innervation of BAT and WAT.[13,14] Specifically, adipocyte regulatory genes have been shown to cooperate with immunological cells to control sympathetic axons, regulating the amount of innervation.[15–17] Consistent with this notion is the discovery of "batokines," which are intrinsic secretory factors from brown adipocytes that can foster changes in angiogenesis, lipid trafficking, neurite growth, and immunometabolism.[18] Collectively, these studies posit that brown adipocytes can coordinate with local niche cells to facilitate or augment brown adipocyte function and thermogenic properties. However, can niche cells influence BAT neurovascular infiltration to control BAT homeostasis and thermogenesis? Indeed, recent evidence suggests that macrophages can stimulate thermogenic fat innervation.[19–23] Nevertheless, the molecular spectrum controlling sympathetic innervation of thermogenic tissue and the regulatory cell types remain to be fully determined and elucidated.

Here, we investigated the functional role of BAT-resident vascular smooth muscle cells (SMCs) to regulate sympathetic innervation and brown adipocyte thermogenesis. We find that SMCs marked by alpha-smooth muscle actin (*Sma*; *Acta2*) do not generate brown adipocytes but rather support the BAT thermogenic niche. Mechanistically, we find that Sma-positive cells produce Cxcl12 to increase $CD301^+$ macrophage accrual and to support basal sympathetic tone, which suppresses lipid accumulation and fosters energy burning. Collectively, the data identify the requirement of SMCs to act as a thermogenic rheostat to provide BAT thermogenic plasticity.

RESULTS

SMC presence is required for BAT lipid homeostasis

SMCs support vascular growth and maintenance and function as discrete tissue progenitors to maintain organ homeostasis and regeneration.[24,25] For instance, a subset of SMCs can function as brown adipocyte precursors.[26] Yet, not all brown adipocyte progenitors are SMCs. For example, SMCs marked by smooth muscle actin (Sma) and myosin heavy chain-11 (Myh11) do not generate brown adipocytes (Figure 1A).[27–29] Thus, can non-adipogenic SMCs support BAT homeostasis? To test this, we designed a mouse model to broadly deplete SMCs by combining the Sma-Cre^{ERT2} mouse model with the diphtheria toxin A (DTA) model (DTA^{Sma}) (Figure 1B).[30,31] We further combined the Sma-Cre^{ERT2} models with the complementary indelible reporter system $Rosa26^{tdTomato32}$ to identify and track Sma-labeled cells. To induce recombination and deplete Sma^+ cells, we administered one dose of tamoxifen (TMX; 50 mg/kg) for 2 consecutive days to control (*Sma-Cre^{ERT2}; Rosa26^{tdTomato}*) and DTA^{Sma} mice (Figures 1B and S1A).[28] At pulse (7 days post-TMX administration), we found, by flow cytometric analysis, a 75% reduction in the number of $Sma^{tdTomato+}$ cells within interscapular BAT (iBAT) from DTA^{Sma} mice (Figure 1C). Notably, at pulse, both control and DTA^{Sma} had comparable iBAT weights (Figure S1B). Correspondingly, iBAT morphology and brown adipocyte gene expression were comparable between control and DTA^{Sma} models (Figures S1C and S1D). Nevertheless, after a 6-week chase (Figure 1B), we observed that DTA^{Sma} iBAT was significantly smaller than controls (Figures 1D and 1E). Importantly, iBAT Sma^+ SMCs remained depleted after the

6 weeks, suggesting limited SMC renewal (Figure S1E). Histologically, DTA^{Sma} iBAT sections displayed unilocular brown adipocytes and had increased lipid droplet area (Figures 1F and 1G). Triglyceride analysis confirmed more lipids within DTA^{Sma} iBAT than in controls (Figure 1H). Increased lipid levels within DTA^{Sma} iBAT were associated with reduced thermogenic regulatory genes (Figure 1I). In addition, Ucp1 immunostaining of DTA^{Sma} iBAT sections revealed a diminished and patchy expression pattern (Figure 1J). To assess whether this directly affected brown adipogenesis, we isolated iBAT stromal vascular (SV) cells from control and DTA^{Sma} mice (Figure S1F). Regardless of genotype, control and mutant brown adipocyte progenitor cells (APCs) had equivalent brown adipocyte differentiation (Figures S1F–S1H). Overall, these data suggest that depleting Sma^{+} cells can promote an increase in iBAT lipid accumulation independent of adipogenic potential.

The cell-killing strategy supports an SMC-specific defect in BAT morphology, but brown adipocyte lipid accumulation may be secondary to WAT dysfunction.[27] While we did not observe a reduction in non-adipose organ weight, subcutaneous and visceral WATs were reduced (Figures S1I and S1J).[27] Non-significant changes in organ weight could be attributed to a renewal of Sma^{+} SMCs throughout the 6-week time frame (Figure S1K). Similarly, we did not observe changes in serum triglyceride levels, hepatic lipid accumulation, or skeletal muscle shivering gene expression in DTA^{Sma} mice (Figures S1L–S1N). To disassociate WAT dysfunction from SMC BAT presence, we combined the Sma-Cre^{ERT2} with the Pparγ$^{fl/fl}$ mouse model (Pparγ^{SMA}; Figure S1O). In this model, Sma^{+} APCs would be rendered non-adipogenic, leading to WAT dysfunction and the potential for BAT lipid spillover, but would maintain SMC presence within iBAT.[27] We induced Pparγ deletion by TMX administration, and mice were phenotypically evaluated 6 weeks later (Figure S1O). In agreement with our previous study,[27] Pparγ mutant mice had reduced WAT (Figure S1P). Yet, serum triglyceride levels and liver lipid accumulation were unchanged (Figures S1Q and S1R). Importantly, SMC-induced Pparγ deletion did not impact iBAT weight, thermogenic gene expression, iBAT lipid accumulation, or iBAT morphology (Figures S1S–S1V). Thus, these findings support that SMCs serve as a functional niche to license brown adipocyte identity.

SMC presence is required for BAT thermogenesis

Because depleting Sma^{+} SMCs promoted iBAT atrophy and whitening, we evaluated if ablating Sma^{+} cells altered brown fat thermogenesis. Toward this end, we acutely (24 h) exposed TMX-induced (6 weeks post-TMX) control and DTA^{Sma} mice to cold temperatures (6.5°C), a time frame in which iBAT is thermogenically activated but not beige fat (Figure 1K).[33,34] Notably, DTA^{Sma} mice could not defend their body temperature in response to cold temperature (Figure 1L). After cold exposure, DTA^{Sma} iBAT weighed less and histologically contained more unilocular adipocytes than control iBAT (Figures 1M–1O). Moreover, Ucp1 and other thermogenic genes were dampened within DTA^{Sma} iBAT samples after cold exposure (Figure 1P). Thus, Sma^{+} SMCs may be critical for maintaining cold-induced thermogenic responses.

BAT SMCs express Cxcl12

To gain mechanistic insight into how SMCs might regulate BAT biology, we evaluated gene expression profiles of several pro- and anti-inflammatory cytokines (Figure 2A). Interestingly, under DTA^{Sma} conditions, the chemokine C-X-C motif chemokine ligand 12 (Cxcl12) was downregulated (Figure 2A). Changes in Cxcl12 abundance have been shown to modulate glucose homeostasis within white adipocytes.[35,36] However, gene expression and functional tests for Cxcl12 within BAT are lacking. To define Cxcl12 expression within iBAT, we employed the $Cxcl12^{DsRed}$ knockin mouse model (Figure 2B). In this model, the fluorescent marker DsRed is reliably expressed from the endogenous Cxcl12 promoter, reporting on active Cxcl12 expression.[37] Based upon whole-mount immunofluorescence, immunostaining of iBAT sections, and *in vitro* adipogenesis, the DsRed signal remained undetectable within brown adipocytes (Figures 2C–2E). Moreover, we could not detect the $Cxcl12^{DsRed}$ signal in isolated floated brown adipocytes (Figure S2A). In agreement, Cxcl12 mRNA expression was enriched within the iBAT SV fraction (SVF) but not the brown adipocyte fraction (Figure S2B). Next, we investigated if Cxcl12 administration could impact brown adipocyte development *in vitro*. However, adipogenesis remained equivalent between vehicle- and recombinant murine Cxcl12 (rmCxcl12; 50 ng/mL)-treated cultures (Figures 2F and 2G). While our data suggest that Cxcl12 may not be involved in brown adipogenesis per se, iBAT Cxcl12 gene expression was upregulated after acute cold exposure, indicating that Cxcl12 within parenchymal cells is responsive to temperature fluctuations (Figure S2C).

Whole-mount $Cxcl12^{DsRed}$ reporter imaging revealed a distinct vascular appearance within iBAT (Figure 2C). Indeed, Sma immunostaining of iBAT sections from $Cxcl12^{DsRed}$ mice revealed colocalization between the DsRed reporter and SMCs (Figure 2E). Moreover, flow cytometric analysis revealed that ~40% of Sma SMCs were also $Cxcl12^{DsRed}$ positive (Figures 2H–2J). Next, we asked if iBAT SMCs distinctly express Cxcl12. Consistently, we found that ~60% of $Cxcl12^{DsRed}$-iBAT SV cells were Sma positive. In contrast, we observed significantly less overlap in other tissues, such as WAT, liver, kidney, spleen, and bone marrow (Figures 2K, 2L, and S2D). We then investigated if $Cxcl12^{DsRed}$ cells were enriched in iBAT compared to other tissues. Interestingly, ~15% of the iBAT SV compartment contained $DsRed^{+}$ cells, which was comparable only to the bone marrow cellular pool (Figure 2M). Similarly, we examined $Cxcl12^{DsRed}$ cell abundance and found that iBAT contained more $Cxcl12^{DsRed}$ cells per tissue weight than other organs (Figure 2N). These data suggest that Cxcl12 may be distinctively enriched within the adult BAT-SMC lineage.

SMC-derived Cxcl12 regulates BAT homeostasis

To determine if SMC-derived Cxcl12 controls BAT function, we combined the $Sma\text{-}Cre^{ERT2}$ mouse model with the $Cxcl12^{fl/fl}$ conditional deletion model[31,38] ($Cxcl12^{Sma}KO$; Figure S2E). We administered TMX to induce Cxcl12 deletion, and mice were chased for 6 weeks and phenotypically evaluated (Figure S2E). Both control and mutant mice gained body weight similarly (Figure S2F). SMCs can serve as WAT progenitors; however, SMC-Cxcl12 deletion did not impact WAT weight or architecture (Figures S2G and S2H). Consistent with intact WAT function, we did not observe ectopic hepatic lipid accumulation or

hyper-triglyceridemia in response to Cxcl12 deletion (Figures S2I and S2J). Interestingly, Cxcl12^{Sma}KO mutant mice developed mild glucose intolerance (Figure S2K). To evaluate if Cxcl12 alters adipogenic potential, we performed *in vitro* adipogenic assays on the isolated SV cell compartment from control and mutant WAT depots. We found that both control and mutant SV cultures had equivalent adipogenesis (Figures S2L–S2N). Overall, it appears that SMC Cxcl12 ablation has limited impact on WAT function.

Upon visual inspection, Cxcl12^{Sma}KO iBAT appeared paler compared to the reddish-brown hue of control iBAT (Figure 3A). Also, Cxcl12^{Sma}KO iBAT was considerably smaller than control iBAT (Figures 3B and S3A). Hematoxylin and eosin (H&E) staining and lipid droplet area quantification of mutant iBAT sections revealed an augmentation in lipid deposition compared to control BAT (Figures 3C, 3D, and S3B). Triglyceride accumulation assessment confirmed elevated lipids within Cxcl12^{Sma}KO iBAT samples (Figure 3E). Moreover, examination of Cxcl12^{Sma} KO auxiliary mouse BAT depots revealed unilocular adipocytes and augmented lipid accumulation (Figures S3C–S3E). Even though lipid accumulation was increased in mutant iBAT, pan-adipocyte genes such as Pparγ, Fabp4, and Plin-1 remained comparable between controls and mutants. In contrast, mRNA expression of brown fat and thermogenic genes was significantly lower in mutant iBAT samples (Figures 3F and 3G). Consistent with mRNA analysis, Cxcl12^{Sma}KO iBAT sections showed a reduction in Ucp1 immunostaining (Figure 3H). Moreover, immunoblotting confirmed a reduction in Ucp1 protein expression within Cxcl12^{Sma}KO iBAT samples (Figure 3I). Also, Cxcl12^{Sma}KO auxiliary BAT depots had lower Ucp1 immunostaining, suggesting overall lower BAT thermogenic potential (Figures S3C–S3E). Consistent with disrupted energy homeostasis, isolated mitochondria from mutant iBAT revealed lower basal and uncoupled respiration rates (Figure S3F). Yet, lower mitochondrial respiration appeared independent of total mitochondrial content (Figure S3G). Collectively, deleting Cxcl12 within SMCs causes BAT atrophy, lowers thermogenic gene expression, and augments brown adipocyte lipid accumulation.

SMC-derived Cxcl12 regulates BAT sympathetic innervation

Comparable brown adipocyte gene expression suggested that the development of brown adipocytes was unaffected by Cxcl12 deletion (Figure 3F). *In vitro* brown adipogenesis further supported this notion, which showed equivalent differentiation between control and mutant cultures (Figures S3H and S3I). Because BAT is densely innervated and sympathetic neurons produce norepinephrine to stimulate lipolysis,[10] we evaluated whether Cxcl12 deletion reduced BAT sympathetic innervation. In agreement with this notion, tyrosine hydroxylase (TH) immunostaining on iBAT sections from TMX-induced control and Cxcl12^{Sma}KO mutant mice (6-week chase) was significantly diminished in Cxcl12^{Sma}KO iBAT sections (Figures 3J and S3J). Furthermore, TH immunoblotting confirmed less sympathetic neuron presence within mutant iBAT (Figure 3K). Reciprocally, immunostaining against TUBB3, a neural-specific tubulin,[39] showed less iBAT innervation in response to Cxcl12 deletion (Figures S3K and S3L). In agreement with less iBAT sympathetic innervation, norepinephrine levels were considerably reduced in Cxcl12^{Sma}KO BAT specimens (Figure S3M). To assess if the lack of sympathetic innervation was related to SMC presence, we performed TH immunostaining on iBAT samples from control and

DTA^{Sma} mice. Indeed, TH immunostaining and immunoblotting revealed significantly lower sympathetic neuron presence within iBAT specimens from the DTA^{Sma} mouse model (Figures 3L, 3M, and S3N). Given that the Sma promoter is active in various SMCs throughout the body, we broadly examined if sympathetic innervation was impaired in other tissues. Foremost, Cxcl12 deletion appeared specific to iBAT, validating our genetic and molecular modeling (Figure S3O). Accordingly, we did not observe changes in TH presence in WAT or heart sections (Figures S3P–S3S). Consistent with a paracrine role for BAT SMC-derived Cxcl12, the circulating levels of Cxcl12 remained similar between control and mutant mice (Figure S3T). Overall, the data suggest that Cxcl12 presence controls sympathetic innervation to coordinate BAT homeostasis.

Loss of Cxcl12 within SMC dampens BAT thermogenesis

Because sympathetic innervation drives BAT thermogenic function, we performed an acute cold tolerance test on TMX-induced control and Cxcl12^{Sma}KO mutant mice (Figure 4A). We found that mutant mice were significantly unresponsive to cold temperatures, as assessed by body temperature defense (Figure 4B). In agreement, metabolic chamber analysis revealed comparable energy expenditure at room temperature, but Cxcl12^{Sma}KO mice displayed a reduction in total energy expenditure throughout the cold challenge (Figure 4C). Consistent with reduced energy utilization, oxygen consumption was less in mutant mice during cold exposure (Figure S4A). However, changes in energy expenditure between control and mutant mice were independent of food intake (Figure S4B). Impaired energetics in cold-exposed mutant mice correlated with minimal induction of Ucp1 and other thermogenic genes (Figures S4C and S4D). In conjunction, Ucp1 immunostaining remained low within cold-exposure Cxcl12^{Sma}KO BAT specimens (Figures S4E and S4F). Consistent with impaired iBAT function, sequential histological sectioning of acute cold-exposed Cxcl12^{Sma}KO mutant iBAT identified the presence of unilocular brown adipocytes (Figure 4D). In support of impaired thermogenic activity, TH immunostaining remained less in mutant iBAT after cold exposure (Figures 4E and S4G). The depressed sympathetic innervation was also observed within iBAT depots of cold-exposed DTA^{Sma} mice (Figures S4H and S4I). These data suggest that Cxcl12^{Sma}KO mice cannot regulate BAT thermogenic function and energy expenditure in response to acute cold-temperature exposure.

The impaired thermogenic response and changes in iBAT morphology and innervation led us to examine whether Cxcl12 directly disrupted brown adipocyte thermogenic capacity. To probe this, we bypassed the cold-induced sympathetic nervous system activation and directly activated brown adipocyte thermogenesis by acutely administering the β3-adrenergic receptor agonist CL316,243 to TMX-induced control and Cxcl12^{Sma}KO mice (Figure S4J).[33,40,41] In response to one injection of CL316,243, we found that brown adipocytes within Cxcl12^{Sma} KO mutant iBAT had reduced lipids and resembled CL316,243-treated control brown adipocytes (Figure S4K). Immunostaining confirmed equivalent CL316,243-induced Ucp1 expression between control and mutant iBAT sections (Figure S4L). In addition, directed qPCR showed comparable CL316,243 induction of Ucp1 mRNA between control and mutant mice (Figure S4M). Next, we took an *in vitro* approach to ask if Cxcl12 directly affects brown adipocyte function. Brown adipocytes from control and mutant mice had similar CL316,243 Ucp1 induction, mirroring our *in vivo* findings (Figure S4N).

Moreover, we found comparable mitochondrial oxygen consumption rates between control and mutant *in-vitro*-derived brown adipocytes stimulated with CL316,243 (Figure S4O). Based on these data, Cxcl12 may function to alter thermogenic activity and lipid catabolism independent of direct brown adipocyte regulation.

Loss of Cxcl12 within SMC promotes diet-induced BAT dysfunction

Defective BAT function is often correlated with susceptibility to diet-induced obesity and metabolic dysfunction.[5,42] Because the data suggest that the loss of Cxcl12 disrupts iBAT homeostasis and thermogenesis, we challenged control and Cxcl12^{Sma}KO mice with a high-fat diet (HFD) for 6 weeks (Figure 4F). HFD feeding did not appear to generate significant differences in body weight or fat content between control and mutant mice (Figures 4G, S4P, and S4Q). However, HFD significantly impaired glucose clearance in Cxcl12-deleted mice compared to HFD controls (Figure 4H). Consistent with the notion that Cxcl12 regulates BAT homeostasis, we observed a significant reduction in Cxcl12^{Sma}KO identifiable iBAT compared to controls (Figure 4I). Histologically, Cxcl12^{Sma} KO brown adipocytes appeared unilocular and enlarged after HFD (Figures 4J and S4R). Consistent with morphological changes, immunostaining showed a reduction in Ucp1 expression within mutant HFD iBAT (Figures 4K and S4S). Cxcl12 deficiency was also associated with reduced anti-inflammatory markers and upregulation of pro-inflammatory genes in response to HFD (Figure S4T). TH immunostaining of iBAT sections from HFD-fed Cxcl12^{Sma}KO revealed reduced sympathetic innervation (Figures 4L and S4U). Overall, the loss of Cxcl12 within SMCs increases susceptibility to HFD-induced changes in BAT morphology and metabolic dysfunction.

SMC-derived Cxcl12 maintains BAT CD301^{+} macrophages

Our data suggest that Cxcl12 regulates BAT homeostasis and sympathetic innervation. While examining Cxcl12^{Sma}KO iBAT histological sections, we noticed an overall reduction in nucleus number compared to control sections (Figures 3C and S5A). This raised the possibility that the loss of Cxcl12 might influence the surrounding niche cells to disrupt BAT metabolism. To delineate relevant mechanisms, we first profiled if the loss of Cxcl12 altered vasculogenic markers within iBAT. Yet, endothelial and SMC markers remained analogous between control and mutant iBAT samples (Figure S5B). Cxcl12 chemokine signaling has been shown to regulate immune cell, macrophage, and monocyte mobilization and retention.[43,44] Toward this end, we evaluated the expression of macrophage and immunological markers between control and mutant iBAT samples. For example, the generalized immunological marker F4/80[45] was considerably lower in mutant iBAT compared to control samples (Figure 5A). In agreement, flow cytometric analysis of mutant BAT samples revealed fewer CD68^{+} macrophages (Figure 5B). Alternatively activated macrophages are often associated with metabolic health and thermogenic function but are frequently disrupted by changes in temperature and diet.[46] In support of this notion, directed qPCR analysis of Cxcl12^{Sma}KO iBAT samples exposed a reduction in anti-inflammatory macrophage markers (Figure 5C).[47] In alignment, flow cytometric analysis indicated a reduction in the abundance of CD301^{+} macrophages in Cxcl12^{Sma}KO iBAT (Figures 5D and S5C–S5E). We also assessed CD301-macrophage presence in the SMC-depleted mouse model, DTA^{Sma}. A reduction in SMC abundance resulted in fewer CD301^{+} macrophages

in iBAT (Figure S5F). Overall, SMC-Cxcl12 deletion is associated with a decline in BAT alternatively activated macrophages.

Cxcl12 drives macrophage accretion to sustain BAT innervation and homeostasis

The data suggest that SMC-Cxcl12 regulates BAT lipid levels, sympathetic innervation, and macrophage accrual; therefore, we probed the progressive order of iBAT decline in response to Cxcl12 deletion. Toward this end, we evaluated control and Cxcl12^{Sma}KO mice at 0, 1, 3, and 6 weeks post-TMX injection for iBAT weight, brown adipocyte lipid accumulation, TH immunostaining, and CD301 macrophage abundance. Interestingly, 1 week post-Cxcl12 deletion, we found that iBAT weight, iBAT morphology, lipid levels, and TH immunostaining remained unchanged compared to TMX-uninduced mice (Figures 5E–5J). Instead, strikingly, we found that CD301^{+} macrophage abundance was significantly reduced in mutant iBAT samples (Figures 5H and 5K). After 3 weeks post-Cxcl12 deletion, iBAT weight did not appear to be significantly different, but Cxcl12^{Sma}KO brown adipocytes had the appearance of lipid accumulation compared to controls (Figures 5E, 5F, and 5I). In addition, we observed a marked reduction in iBAT TH immunostaining and a continued decrease in CD301 numbers (Figures 5G, 5H, 5J, and 5K). At 6 weeks post-Cxcl12 deletion, iBAT weight was lower, CD301^{+} macrophages were reduced, TH presence was diminished, and brown adipocyte lipid accumulation was more significant (Figures 5E–5K). Thus, the loss of Cxcl12 may principally invoke changes in CD301 macrophage presence, precipitating a decline in sympathetic innervation and tone and then facilitating brown adipocyte lipid filling.

Exogenous Cxcl12 restores BAT homeostasis and sympathetic innervation

The data suggest that SMC-derived Cxcl12 may regulate BAT macrophage accrual to support sympathetic innervation and brown adipocyte lipid levels. To test the requirement of Cxcl12 in BAT homeostasis, we administered vehicle or recombinant murine Cxcl12 (rmCxcl12; 100 ng/mouse) protein for 10 consecutive days to TMX-induced control and Cxcl12^{Sma}KO mice (6-week chase) maintained at room temperature (Figure 6A). H&E staining revealed that rmCxcl12 restored the brown adipocyte multilocular appearance within Cxcl12^{Sma}KO iBAT sections (Figure 6B). In confirmation, lipid droplet area quantification and triglyceride analysis indicated that administering rmCxcl12 protein to Cxcl12^{Sma}KO mice normalized lipid levels (Figures S6A and S6B). Notably, treating control mice with rmCxcl12 did not alter the iBAT lipid levels (Figure S6A). Moreover, immunostaining and directed qPCR analysis showed that administering rmCxcl12 increased Ucp1 presence within Cxcl12^{Sma}KO iBAT samples (Figures 6C, S6C, and S6D). In addition, rmCxcl12 administration restored TH^{+} sympathetic neurite projections, suggesting more innervation (Figures 6D and S6E). We also tested if rmCxcl12 could restore iBAT homeostasis in DTA^{Sma} mice (Figure 6A). Indeed, rmCxcl12 restored the histological and molecular profiles of DTA^{Sma} iBAT independent of weight (Figures 6E, S6F, and S6G). For instance, rmCxcl12 increased in Ucp1 and TH immunostaining, suggesting that Cxcl12 can restore thermogenesis and sympathetic innervation within DTA^{Sma} iBAT (Figures 6F, 6G, and S6H–S6J).

Cxcl12 deletion within Sma^+ cells resulted in acute loss of $CD301^+$ macrophages. Consistent with the notion of CD301 cell recruitment, treating $Cxcl12^{Sma}KO$ (1 week post-TMX) mice with rmCxcl12 for 2 days fully restored iBAT CD301 macrophage abundance to control levels (Figures S6K–S6M). In agreement, treating DTA^{Sma} mice with rmCxcl12 restored CD301 iBAT abundance comparable to control levels (Figures S6K, S6N, and S6O), confirming that macrophages are responsive to Cxcl12 bioavailability.

Rodents experience thermal stress at room temperature, masking any potential effect of rmCxcl12 on innervation and lipid accumulation in room-temperature-housed control mice.[48] Accordingly, housing mice at 30°C (thermoneutrality) alleviates cold-induced signals by deactivating adrenergic signaling, allowing BAT to "whiten."[48–50] Therefore, we administered rmCxcl12 protein for 10 days to control mice housed at thermoneutrality for 3 weeks (Figure 6H). Strikingly, treating mice with rmCxcl12 reactivated iBAT by reducing brown adipocyte lipid accumulation and stimulating sympathetic neurite outgrowths (Figures 6I and 6J). Together, these data support the notion that the exogenous Cxcl12 augments BAT homeostasis by promoting CD301 macrophage recruitment and sympathetic innervation.

Cxcl12 supplementation improves obesity-induced BAT dysregulation

Our rmCxcl12 studies suggested that the administration of Cxcl12 could be employed to counteract diet-induced changes in BAT morphology and function. Toward this end, we administered one dose of rmCxcl12 (100 ng/mouse) for 10 consecutive days to HFD-fed obese C57BL/6J male mice (Figure 7A). Treating HFD-fed mice with rmCxcl12 for 10 days did not significantly change body fat, glucose clearance, serum triglycerides, hepatic steatosis, or energy expenditure (Figures S7A–S7E). However, histological staining of iBAT and auxiliary BAT depot sections revealed that rmCxcl12 administration reduced lipid content and restored the multilocular brown adipocyte appearance (Figures 7B, 7D, and S7F). In agreement, we observed increased Ucp1 positivity and thermogenic gene expression after rmCxcl12 administration (Figures 7C, 7E, S7F, and S7G). TH^+ sympathetic neurite presence was also restored after rmCxcl12 delivery (Figures 7F and 7G). In addition, rmCxcl12 increased iBAT $CD301^+$ macrophage abundance (Figure S7H). As a next step, we evaluated if rmCxcl12 administration could increase acute cold temperature sensitivity (Figure 7H). Treating HFD mice with rmCxcl12 improved body temperature defense and increased energy expenditure and oxygen consumption after cold exposure (Figures 7I, 7J, and 7K). Overall, Cxcl12 alleviated diet-induced BAT dysfunction and improved thermogenic responses.

Leptin-deficient (Ob/Ob) mice are obese and hypothermic; therefore, we evaluated if treating Ob/Ob mice with Cxcl12 for 10 days would improve BAT morphology and function (Figure S7I). Strikingly, administration of rmCxcl12 reduced iBAT weight and improved glucose clearance in Ob/Ob mice (Figures S7J and S7K). In addition, there was a reduction in hepatic lipid appearance after rmCxcl12 administration (Figure S7L). Moreover, administration of rmCxcl12 induced iBAT morphological remodeling, which was supported by a marked upregulation of Ucp1 and other thermogenic genes in response to rmCxcl12 treatment (Figures 7L, 7M, S7M, and S7N). Flow cytometric analysis revealed an increase

in iBAT CD301$^+$ macrophage abundance after rmCxcl12 administration (Figure S7O). Enhanced macrophage accrual was associated with an increase in iBAT anti-inflammatory markers in response to rmCxcl12 (Figure S7P). Critically, rmCxcl12 reestablished iBAT TH$^+$ sympathetic projections (Figures S7Q and S7R).

Next, we evaluated if Cxcl12 administration could extend the cold temperature tolerance of Ob/Ob mice (Figure 7N). Indeed, treating Ob/Ob mice with rmCxcl12 increased cold temperature survival compared to vehicle-treated mice (Figure 7O). Moreover, rmCxcl12 increased the presence of Ucp1$^+$ multilocular brown adipocytes within cold-exposed Ob/Ob iBAT (Figures 7P, 7Q, and S7S). Correspondingly, rmCxcl12 boosted the expression of iBAT thermogenic genes (Figure S7T). In addition, we observed that rmCxcl12 administration increased TH sympathetic innervation within cold-exposed Ob/Ob iBATs (Figures S7U and S7V). Administration of rmCxcl12 also boosted CD301-macrophage accretion in cold-exposed Ob/Ob mice (Figure S7W). Together, the data suggest that Cxcl12 can act as a potent inducer of sympathetic innervation and macrophage accrual to control brown adipocyte homeostasis and thermogenic function.

DISCUSSION

In this study, we identify a BAT thermogenic communication network between SMCs, macrophages, and sympathetic neurons that is driven by Cxcl12 signaling. The generation of thermogenic fat cells is clinically desirable due to their ability burn glucose and free fatty acids futilely, generating heat rather than cellular energy.[5] However, a major therapeutic obstacle has been the inability to generate new thermogenic tissue. While the hierarchical understanding of the transcriptional molecular regulators governing the thermogenic process are being defined, less is known regarding the local niche signals acting on thermogenic fat cells.[51–53] Our findings unveil an intricate function of the BAT SMC niche to produce Cxcl12 to support and retain local anti-inflammatory macrophages and maintain essential BAT sympathetic innervation.

The molecular regulation linking anti-inflammatory macrophage accrual to thermogenic adipose tissue has recently drawn attention.[23] Our data support the notion that Cxcl12 signaling mediates, in part, macrophage recruitment to participate in BAT thermogenesis. In agreement with this view, macrophages are recruited to and support sympathetic innervation[9,19]; however, detailed mechanistic insights into how macrophages regulate neurite presence is unclear. Yet, recent work has suggested that Cx3Cr1$^+$ BAT macrophages, a CD301$^+$ macrophage subpopulation, can support BAT innervation by regulating Mecp2, a nuclear transcription regulator often mutated in Rett syndrome.[22,54] Moreover, other factors, such as Slit3, have been shown to regulate sympathetic innervation of brown and beige thermogenic tissue via macrophages.[55] However, the spectrum of key macrophage-derived molecules has not been shown to support sympathetic neurons to maintain BAT homeostasis. Broadly, our studies used systemic treatment of Cxcl12, which could elicit secondary targets in other organs to stimulate macrophage recruitment and activation. It is possible that Cxcl12 may regulate macrophage accrual within other organs to control tissue homeostasis and metabolic function.[56] This could imply that Cxcl12 may remodel whole-body immunological cell composition, affecting several metabolic diseases. Interestingly,

our study unravels an even deeper layer of complexity between BAT SMCs and temperature fluctuations to coordinate macrophage recruitment and retention. This may suggest the broader function of vascular resident cells within BAT or other tissues.[25,57] In addition, more evidence of changes in other BAT niche cells could provide new inroads into brown adipocyte thermogenesis and function.[58]

The generation and activation of thermogenic fat is considered to protect humans from obesity.[59,60] Indeed, treating diet- or genetically induced obese mice with Cxcl12 boosts BAT function and thermogenesis. For that matter, mice lacking Cxcl12 with SMCs are susceptible to diet-induced BAT and metabolic dysfunction. However, the role of SMCs and Cxcl12 in human BAT remains unexplored. The use of single-cell transcriptomics may tease apart populations in human thermogenic tissue that resemble mouse SMC Cxcl12^{+} populations.[34,61–63] Furthermore, BAT atrophy is observed in aging humans and rodents[64–66]; however, the mechanisms of BAT perdurance remain largely unexplored.[67] Future investigation into the Cxcl12 regulatory pathways could be beneficial for understanding the age-dependent decline in BAT. Nevertheless, this study establishes a previously unrecognized homeostatic function of SMCs to regulate the bioavailability of Cxcl12 to retain a subset of macrophages, support BAT innervation, and allow thermogenic plasticity. Altogether, the data suggest that maintaining supportive BAT macrophages via Cxcl12 signaling could be a beneficial mechanism for brown adipocyte perdurance and metabolic homeostasis.

Limitations of the study

Although our study reveals the importance of SMC-derived Cxcl12 in regulating BAT sympathetic activity and macrophage accrual, several limitations exist. We exclusively used male mice for BAT thermogenic-SMC-macrophage modeling. This was an attempt to diminish the effect of estrogen signaling on BAT thermogenic activity. Future studies examining male and female subjects will provide insight into varying thermogenic-SMC-macrophage circuits. Moreover, prospective studies focusing on macrophage-specific Cxcl12-Cxcr4 signaling will expose the potential molecular mechanisms and by-products stimulating BAT sympathetic innervation. In addition, our study emphasized the role of SMC Cxcl12 within BAT, yet the potential contribution of Cxcl12 to subcutaneous WAT beige fat biogenesis should be explored.

STAR★METHODS

RESOURCE AVAILABILITY

Lead contact—Further information and requests for resources and reagents should be directed to and will be fulfilled by the lead contact, Daniel C. Berry, Ph.D., Division of Nutritional Sciences, Cornell University, Ithaca, NY 14853 USA (mailto:dcb37@cornell.edu).

Materials availability—This study did not generate unique reagents.

Data and code availability

- All data reported in this paper will be shared by the lead contact upon request.
- This paper does not report original code.
- Any additional information required concerning the data reported in this paper is available from the lead contact upon request.

EXPERIMENTAL MODEL AND SUBJECT DETAILS

Animals—All animal experiments were performed according to procedures approved by the Cornell University Institutional Animal Care and Use Committee under the auspices of protocol 2017–0063. Mice were maintained on a 14:10-hour light/dark cycle with free access to food and water. All animal experiments were performed on 3 or more mice per cohort and performed at least twice. Sma-Cre^{ERT2} mouse model was generously obtained from Drs. Pierre Chambon and Daniel Metzger[31]. R26$^{-tdtomato}$ (stock #007914), R26^{-DTA} (stock #009669), Cxcl12$^{fl/fl}$ (stock #021773); Cxcl12^{DsRed} (stock #022458), and Ppar$\gamma^{fl/fl}$ (stock # 004584) were purchased from Jackson Laboratories. Offspring were intercrossed for six generations and were maintained on mixed C57BL6/J-129SV background to generate experimental models. All experiments were performed on two-month-old (P60) male mice unless specified. To induce recombination, the mice were administered one dose of TMX (50 mg/Kg; Cayman Chemical: 13258) dissolved in sunflower seed oil (Sigma, item no: S5007) for two consecutive days via intraperitoneal (IP) injection. After the final TMX injection, mice were maintained for various time points (0, 1, 3, or 6 weeks) at room temperature (~23°C) prior to experimentation. For temperature exposures, mice were housed in a 6.5°C (cold exposure) or 30°C (thermoneutral) rodent incubation chamber (Power Scientific RIS70SD).

METHOD DETAILS

Physiological measurements—Temperature was monitored hourly or daily using a TH-5 Thermometer (Physitemp) attached to a RET-3 rectal probe for mice (Physitemp). Prior to insertion, the probe was lubricated with glycerol and was inserted 1/2 inch and temperature was measured once stabilized. Glucose monitoring: blood glucose levels were measured with a Contour glucometer (Bayer) and with Contour glucose strips.

Metabolic cage analysis—Mice were singly housed and acclimated for two days at room temperature (23°C) in a Promethion metabolic screening system prior to data collection. Cages are equipped with food hoppers, water bottles, and elevated shelter huts for continuous body weight and food and water intake monitoring. Cages are housed in an environmentally controlled cabinet, measuring oxygen consumption, carbon dioxide production, food intake, and total locomotor activity to calculate the respiratory exchange ratio and total energy expenditure. After the acclimation period, data was recorded for 48 hours at room temperature. Mice were then taken out of the cages, and the chamber was then chilled to 6.5°C for cold temperature measurements. Mice were kept at 6.5°C and data recorded for 24 hours in the cold. Data analysis was conducted using the web based indirect calorimetry software CalR[68].

Pharmacological treatments—For rmCxcl12 treatments, mice at the denoted time points were administered one dose of vehicle (1X PBS with 1% BSA) or one dose of recombinant Cxcl12 (100 ng/mouse; PeproTech: 250–20A) dissolved in 1X PBS with 1% BSA for ten consecutive days via IP injection. For CL316,243 treatments, mice were administered one dose of vehicle (1X PBS) or one dose of CL316,243 (1 mg/kg; 17499 Cayman Chemicals) by IP injection for 24 hrs.

Immunofluorescence staining—Tissues were dissected from mice and submerged in 10% formalin solution, diluted with 1X PBS, for at least 24 hours. These tissues were then processed utilizing Thermo Scientific™ STP 120 Spin Tissue Processor: 50% ethanol for 45 minutes, 70% ethanol for 45 minutes, 80% ethanol for 45 minutes, 95% ethanol for 45 minutes (2x), 100% ethanol for 45 minutes (2x), Xylene Substitute for 45 minutes (3x), paraffin for 4 hours (2x). After processing, tissues were embedded into cassettes using a Histostar™ embedding station. Tissues refrigerated at 4°C for 24 hours prior to sectioning. Low profile blades were used to collect 8–40 μm sections for BAT and 8–12 μm sections for iWAT (inguinal WAT) using a HM-325 microtome. Tissue-slides were baked overnight at ~55°C. Slides were then rehydrated: xylene for 3 min (3x), 100% ethanol for 3 min (2x), 95% ethanol for 3 min (2x), 70% ethanol for 3 min, 50% ethanol for 3 min, running dH_2O for 30 seconds, 1X PBS for 10 minutes. Slides were submerged in 1X Citrate Buffer from 10X stock solution (Electron Microscopy Sciences R-Buffer A, 10X, pH 6; Catalog: 62706–10) and placed in the Antigen Retriever (Electron Microscopy Sciences) filled with 750 mL of dH_2O and processed for 2 hours. Slides were placed in 1X PBS for 15 minutes and dried thoroughly with Kimwipes and ImmEdge™ Pen (Vector Laboratories; Catalog: H-4000).

For BAT, slides washed in 1X TBS for 5 minutes (3x), and 0.3% Triton X-100 with 1X TBS. Slides were left in Triton X-100 (0.3%) overnight to permeabilize. Slides were washed with 1X TBS for 5 minutes and then blocked with 5% donkey serum (Sigma #D9663) for 30 minutes, washed with 1X TBS for 5 minutes and then enclosed with primary antibody in 1X TBS refrigerated overnight. The primary antibodies in this experiment are as follows: anti-Tubulin Beta 3 (1:200; 657404 BioLegend), goat anti-Perilipin (1:200; abcam: ab61682), rabbit anti-Ucp1 (1:200; abcam: ab10983), mouse anti-Caveolin-1 (1:200; Novus: (7C8) NB100–615), Human/Mouse/Rat alpha-Smooth Muscle Actin Antibody(1:100, R&D Systems: MAB1420). Afterwards, the slides were washed with 1X TBS for 10 minutes and loaded with the appropriate secondary antibody from the following for 2 hours at RT: Texas Red donkey anti-rabbit (1:200; ThermoFisher Scientific: Alexa Fluor 568 A10042), 488 donkey anti-goat (1:200), Cy5 donkey anti-mouse (1:200; Jackson ImmunoResearch 715–175-150). Fluorescent images were obtained on a Leica DMi8 inverted microscope system.

For TH staining in BAT, 40-micron sections were collected, baked, rehydrated, and antigen retrieval was performed as described above. Slides were then permeabilized in 1 X PBS/ 0.2% Triton X-100/20% DMSO/0.3 M glycine at 37°C overnight. Slides were then blocked in 1X PBS/0.2% Triton X-100/10% DMSO/5% donkey serum at 37°C overnight. Tissues were then incubated with primary antibody- rabbit anti-tyrosine hydroxylase (TH) (1:200; EMD Millipore: ab152)- diluted in 1X PBS/0.2% Tween-20/5% DMSO/5% donkey serum

at 37°C for 48 hrs. Slides were then washed 3x and secondary antibody- Texas Red donkey anti-rabbit (1:200; ThermoFisher Scientific: Alexa Fluor 568 A10042)- diluted in 1X PBS/0.2% Tween-20/5% DMSO/5% donkey serum was then applied for 2 hours at room temperature. Slides were then washed 3x and .3% Sudan black was applied for 3 minutes. Slides were then washed 3x and cover slipped. Fluorescent images were obtained on a Zeiss LMS710 microscope.

For TH staining in iWAT and heart, slides were left to permeabilize overnight in 1x TBS-Triton X-100 (0.3%). Slides were washed with 1X TBS for 5 minutes and then blocked with 5% donkey serum for 30 minutes. Wash step was repeated, and slides were enclosed in primary antibody to refrigerate for 36 hours. Slides were washed with 1x TBS for 1 hour. Secondary antibody was loaded onto the tissue for 4 hours at RT and washed with 1X TBS for 10 minutes. Tissues were exposed to 0.1% Sudan Black in 70% ethanol for 5–10 minutes, washed with 1X TBS for 10 min (3x), and covered with 0.02% Tween20 in 1X TBS for 15 minutes. Tissue was washed with 1X TBS for 10 minutes and stained with Hoescht in 1X TBS (1:1000; H3570; Life Technologies) for another 10 minutes and then washed again with 1X TBS for 5 minutes. Fluorescent images were obtained on a Leica DMi8 inverted microscope system.

RNA isolation and qPCR—~200 mg of BAT or iWAT tissue were randomly selected from each group and placed into Precellys tubes that included ceramic beads and 1mL of TRIzol (Ambion #15596018). Samples were placed into a Precellys 24 Lysis and Homogenization machine (Bertin Technologies) to homogenize and set at three pulses at 4500 rpm (30 sec) with 30-second rest periods between each pulse and a final rest period of 4 minutes. For cell culture experiments, cells were directly disassociated with TRIzol. RNA was collected using the Chloroform extraction and isopropanol precipitation procedure. A TECAN Infinite F-Nano+ spectrophotometer determined the RNA concentrations. RNA samples were converted into cDNA utilizing a high-capacity RNA to cDNA kit (Life Technologies #4368813) and placed in a thermal cycler. The converted sample was diluted (1:10) for qPCR analysis. The diluted cDNA sample was mixed with PowerUp™ SYBR™ Green Master Mix (Life Technologies A25742) and the necessary primer (Table S1). Samples were placed into an Applied Biosystems QuantiStudio™ 3 Real-Time PCR system for qPCR analysis. The machine was set to collect data using the ΔΔ-CT method compared to the internal control Rn 18s. Each datum corresponds to a single mouse sample/culture and was executed in technical quadruplets.

Mitochondrial isolation and respiration assay—Freshly dissected BAT from mice were homogenized with cold respiration buffer (2.5 mM glucose, 2.5 mM sodium pyruvate, 1 mM malate, 120 mM NaCI, 4.5 mM KCI, 0.7 mM Na_2HPO4, 1.5 mM NaH_2PO_4 and 0.5 mM $MgCl_2$, pH 7.4)[69] at 5–7 pulses using a tightly fitted dounce homogenizer. The homogenized solution was filtered through a 100-micron mesh and then centrifuged at 600xg for 10 minutes at 4°C[70]. The resulting supernatant was collected into a separate tube and centrifuged at 8500xg for 10 minutes at 4°C. The formed pellet, containing the mitochondria, was resuspended gently in 200–300 μL of respiration buffer and quantified through a Pierce BCA Protein Assay Kit (Cat: 23225) following manufacturer's protocol.

Mitochondria were plated in an Agilent Seahorse XF24 Cell Culture Microplate at 10 μg per well. Wells were filled to 50 μL with respiration buffer and spun at 2000xg for 20 minutes at 4°C. Each well was then filled with prewarmed respiration buffer (37°C) to a final volume of 500 μL per well. Mitochondrial respiration was measured using an Agilent XFe24 Analyzer following the manufacturer's guidelines. Oligomycin (thermoscientific Cat: J61898.MA) was loaded into the cartridge port at 10X to reach a final concentration of 4 μM in the respiration buffer.

For brown adipocytes, primary cells were isolated and differentiated as described below. After differentiation, cells were washed (2x) in pre-warmed (37°C) Seahorse XF DMEM Medium (pH = 7.4) supplemented with 10 mM glucose, 1mM sodium pyruvate, 2mM L-glutamine. After the final wash, cells were incubated in a non-CO_2 37°C chamber for 1 hour. After incubation, cells received fresh medium at a final volume of 500 μL per well. CL316,243 was loaded into the cartridge port at 10X to reach a final concentration of 10 mM in the medium. Agilent Wave™ software was used to determine OCR measurements and statistical analyses.

Mitochondrial DNA extraction—A modified protocol was used as previously described[71,72]; freshly isolated mouse BAT was homogenized to a pellet as described above. The mitochondrial pellet was resuspended in 100 μl resuspension buffer (10 mM Tris, 0.15 M NaCl, 10 mM EDTA, pH 8) for immediate DNA extraction. For DNA extraction, 200 μl of alkaline lysis buffer (0.18 N NaOH, 1% SDS) was added, followed by incubation on ice for 5 minutes. Subsequently, 150 μl of potassium acetate buffer was added, gently vortexed, and placed on ice for another 5 minutes. After centrifugation at 12,000xg for 5 minutes at 4°C, the supernatant was transferred to a new tube. RNase (1 μg) was added, and the mixture was incubated at room temperature for 10–20 minutes. A phenol-chloroform extraction was performed, followed by ethanol precipitation with 40 μl of sodium acetate (3M), 1 μl of glycogen (20 mg/ml), and 1,200 μl of 100% ethanol. After washing the DNA pellet with 70% ethanol and air-drying, the pellet was resuspended in low TE Buffer (10 mM Tris-HCl, 0.1 mM EDTA, pH 8) for quantitative analysis. DNA quality and quantity were assessed by TECAN infinite F-nano$^+$ spectrophotometer.

Norepinephrine quantification—BAT was dissected, weighed, and flash frozen in liquid nitrogen. Frozen tissue was then homogenized using a Spectrum Labs Bessman Tissue Pulverizer and resuspended in .5 ml of .1 M Trichloroacetic acid, 10.5 % Methanol, 10^{-2} M Sodium Acetate, and 10^{-4} M EDTA. Samples were then spun at 10,000xg for 5 minutes. The supernatant was then collected and washed with 1:1:2 water, chloroform, and methanol to remove any residual lipid. The supernatant was then collected and evaporate to 200 uL in a Thermofisher Speed Vac Savant DNA120. The neurotransmitters and their metabolites were then measured by liquid chromatography tandem mass spectrometry (LC-MS/MS) as described[73] with modifications based on our instrumentation and the addition of internal standards. The system (Thermo Finnigan) included a TSQ Quantum Access mass spectrometer with an electrospray ionization source, and a Dionex UniMate 3000 UPLC system (Thermo). The separation of the compounds was achieved using a Phenomenex Luna C18(2) analytical column (250 × 4.6 mm, 5 mm) and matching guard column. The mobile

phase consisted of 0.02% formic acid in water and 0.02% formic acid in acetonitrile with gradient elution. The flow rate was 500μL/minute, the injection volume was 10μL and the column temperature was maintained at 25°C. Norepinephrine and norepinephrine D6 were detected in positive ionization mode. The parent ion/daughter ion fragments monitored were m/z 170/152 (norepinephrine), m/z 176/158 (norepinephrine-2,5,6,α,β,β-D6). Samples were analyzed using Xcalibur Software (Thermo).

Western blot/immunoblotting—BAT and adrenal gland samples were randomly selected and homogenized using 200 μL RIPA Lysis Buffer. Standard curve and relative protein concentrations for samples were determined utilizing the protocol provided in a protein assay kit (Pierce™ BCA Protein Assay – ThermoScientific #23225). Samples were then prepared utilizing calculated protein concentrations with SDS/DTT (1:1 ratio) in 10% Mini-PROTEAN TGX Gel (BioRad #4561034). The gel was placed into a Mini-PROTEAN Tetra Electrophoresis Cell chamber suspended in 1X TRIS-Tricine-SDS running buffer (ThermoScientific #J60992.K2). Samples were then run for 15–20 minutes at 90V followed by 120V for 2 hours with Precision Plus Protein Dual Color Standards protein ladder (BioRad #1610374). Gel was then transferred with 1X Tris/Glycine Buffer (BioRad #1610771) onto Immobilon-P^{SQ} Transfer membrane (Millipore #ISEQ00005) overnight at 30V. Membrane was washed with 1x TBS-0.1% Tween20 (TBS-T) 4x for 5–10 minutes each time on a rocker. Membrane was then blocked with 5% BSA (FisherScientific #BP1600–100) in 1X TBS-T for 1 hour, washed 4x for 5–10 minutes in 1x TBS-T and loaded with the appropriate primary antibody overnight on rocker overnight in cold room. The primary antibodies in this experiment are as follows: rabbit anti-Ucp1 (1:1000; abcam #ab10983); rabbit anti-tyrosine hydroxylase (1:1000; EMD Millipore: ab152); rabbit anti-beta-tubulin (1:1000; Cell Signaling: 15155); rabbit anti-GAPDH (1;1000; Cell Signaling: 2118). Membrane was washed again 4x in 1x TBS-T for 15 minutes and covered in secondary antibody for 1 hour (1:10000; ThermoFisher Scientific: donkey anti-rabbit IgG (H+L) Cross-Adsorbed HRP 31458). Membrane was washed as previously mentioned and submerged in 1:1 solution of SuperSignal™ West Pico PLUS Chemiluminescent Substrate (ThermoScientific: 34580) for 1 minute and developed utilizing a FlourChem E system (bio-techne® proteinsimple).

Image quantification

TH and UCP1 fluorescence quantification: Fiji ImageJ software was used to quantify percent fluorescent intensity of tyrosine hydroxylase and UCP1 over total fluorescent signal. Color thresholds were adjusted to highlight specifically tyrosine hydroxylase or UCP1 emission on their individual fluorescent channels and utilized to calculate average fluorescent intensity percentages among respective experimental groups. Three images per mouse for three mice per group were quantified.

Adipocyte quantification: Fiji ImageJ Adiposoft plugin was utilized to highlight and quantify individual adipocyte areas from respective H+E images. All values are represented in um^2. Three images per mouse for three mice per group were quantified.

SV cell isolation from adipose and non-adipose tissue

WAT SVF isolation: Fat pads were removed and a pair of inguinal adipose depots from a single mouse were minced and placed in 10 ml of isolation buffer (0.1 M HEPES, 0.12 M NaCl, 50 mM KCl, 5 mM D-glucose, 1.5% BSA, 1 mM CaCl2) supplemented with collagenase type I (10,000 units) and incubated in a 37°C incubator with gentle agitation for ~1 hour [74]. Serum free Dulbecco's Modified Eagle's Medium Nutrient Mixture F-12 Ham (Sigma, cat. no. D8900 and D6421) (DMEM/F12) media was added to the digested tissue and strained through a 100 μm cell strainer. Samples were spun (Eppendorf at 200xg for 10 minutes. The supernatant was removed, and the pellet was resuspended in 10 ml of erythrocyte lysis buffer (155 mM NH4Cl, 10 mM KHCO3, 0.1 mM EDTA). After a 5-minute incubation period, growth media (DMEM/F12 supplemented with 10% fetal bovine serum (FBS) was added, mixed, and strained through a 40 μm cell strainer. Samples were then spun at 200xg for 5 minutes. Supernatant was removed and the cell pellet was resuspended growth media and cells were plated. After ~12 hours, growth media was removed and replenished.

BAT SVF isolation: Mice were dissected, and SV cells were isolated from brown fat lobes. Briefly, tissue was minced and digested for half an hour with vortexing every ten minutes in 5 ml isolation buffer containing collagenase II (50,000 units) at 37°C. 5 ml DMEM/F12 was then added, and the suspension filtered through a 70 μm basket. Suspension was then spun at 200xg for 10 minutes and the supernatant aspirated off. The pellet was then resuspended in 10 ml erythrocyte lysis buffer (155 mMNH4Cl, 10 mMKHCO3, 0.1 496mM EDTA) for 5 minutes. 15 ml of DMEM/F12 supplemented with 10% FBS was added, the suspension filtered through a 40 μm basket, and spun at 200xg for 5 minutes. Isolated SV cells were resuspended and cultured in DMEM/F12 supplemented with 10% FBS. The following day, growth media was removed and replenished.

Organ SVF isolation: Respective organs (liver, kidney, and spleen) were removed and weighed prior to cell isolation. Tissue was minced and placed in 10 ml of isolation buffer (0.1 M HEPES, 0.12 M NaCl, 50 mM KCl, 5 mM D-glucose, 1.5% BSA, 1 mM CaCl2) supplemented with collagenase type I (10,000 units) and incubated in a 37°C incubator with gentle agitation for ~1 hour. Samples were additionally vortexed every ten minutes to assist digestion. Serum free Dulbecco's Modified Eagle's Medium Nutrient Mixture F-12 Ham (Sigma, cat. no. D8900 and D6421) (DMEM/F12) media was added to quench the digestion and the suspension strained through a 100 μm cell strainer. Samples were then spun at 200xg for 10 minutes. The supernatant was removed, and the pellet was resuspended in 10 ml of erythrocyte lysis buffer (155 mM NH4Cl, 10 mM KHCO3, 0.1 mM EDTA). After a 5-minute incubation period, growth media (DMEM/F12 supplemented with 10% fetal bovine serum (FBS) was added, mixed, and strained through a 40 μm cell strainer. Samples were then spun at 200xg for 5 minutes. Supernatant was removed, and the cell pellet was resuspended for flow cytometric analysis.

Bone marrow isolation: For bone marrow analysis, the femur bones of mice were dissected out, and all muscle was removed. Each end of the femur was then cut with sterile scissors. An 18-gauge needle was then used to create a small hole in a 0.5 ml microcentrifuge

tube. Femurs were then placed into their respective .5 ml tube and nested into a 2 ml microcentrifuge tube. Samples were then spun at 10,000xg for 30 seconds to flush out the bone marrow. The cell pellet was then resuspended in 1 ml of RBC buffer for 5 minutes at room temperature. 5 ml of growth media supplemented with 10% FBS was then added and strained through a 40 μm cell strainer. Samples were then spun at 500xg for 5 minutes. Supernatant was removed, and the cell pellet was resuspended for flow cytometric analysis.

Adipogenesis

White fat adipogenesis: Isolated SV cells were resuspended and culture in DMEM/F12 supplemented with 10% FBS. The following day, media was removed and replenished, and cells were grown to confluency. To induce adipogenesis, confluent cells were treated with differentiation media one: DMEM/F12 containing 5% FBS, insulin (10 μg/mL), dexamethasone (5 mM), and isobutylmethylxanthine (0.5 mM). After 72 hours, adipogenic media one was removed and differentiation media two: DMEM/F12 containing 5% FBS and insulin (10 μg/mL). Adipogenesis was assessed via LipidTox staining.

Brown fat adipogenesis: Isolated SV cells were resuspended and cultured in DMEM/F12 supplemented with 10% FBS. The following day, growth media was removed and replenished. Cells were grown to confluency and brown fat adipogenesis was induced by treating confluent cells with DMEM/F12 containing 5% FBS, insulin (10 μg/mL), dexamethasone (5 mM), isobutylmethylxanthine (0.5 mM), 2 nM Triiodothyronine (T3) and 250 nM Indomethycin. At 72 hours, differentiation mix one was removed and differentiation media two (DMEM/F12 supplemented with 5% FBS; 10 ug/ml insulin, 2nM T3, and 250 nM Indomethycin) was added for the remainder of the differentiation process. Adipogenesis was assessed via LipidTox staining. To activate brown adipocytes, cells were exposed to 1 μm CL316,243 for 24 hrs. and subsequently harvested or analyzed.

LipidTox staining—At the end of differentiation, media was aspirated, and adipocytes were fixed with 4% paraformaldehyde for 45 minutes. Adipocytes were washed thrice with 1xTBS with a 5-minute incubation between each wash. Adipocytes were permeabilized using 0.3% TritonX-100 in 1XTBS for 30 minutes. Adipocytes were washed as previously described. Adipocytes were incubated with either HSC LipidTox-green or HSC LipidTox-deep red at 1/1000 in 1xTBS. Adipocytes were then washed twice with 1xTBS with a 3-minute incubation between each wash. Adipocytes were then stained with Hoechst (1 μg/ml in 1XTBS) for 10 minutes. Adipocytes were washed twice with 1xTBS with a 3-minute incubation between each wash. Fluorescent images were collected on a Leica DMi8 inverted microscope system.

Flow cytometry—White and brown adipose cells were isolated as previously described[75,76]. Cells were resuspended in 1X PBS. Cells were then pelleted (200xg for 10 minutes) and resuspended in 0.3–0.5 ml of FACS buffer (2% Fetal Bovine Serum; 2 mM EDTA in 1xPBS with 1X phosphatase inhibitor cocktail) and pipetted through 5 ml cell-strainer capped FACS tube (BD Falcon). Cell sorting was performed on a BD Biosciences FACS Aria Fusion. Cells were analyzed on a Thermo-Fisher Attune NxT cytometry. Viable cells were gated by singlet forward and side scatter pattern and GFP+ and RFP+ viable

cells were either analyzed or sorted. Alternatively, cells were stained for CD45 (1:200; 103151 Biolegend), CD301 (1:200 145705 Biolegend), or CD68 (1:200 137003 Biolegend) antibodies and analyzed for their respective conjugated fluorophore.

Blood and tissue chemistry assays—Blood was randomly collected via a cardiac puncture. Blood was allowed to coagulate for 2–3 hrs and subsequently spun at 7,500 rpm for 5 minutes and serum was collected. Serum and BAT triglyceride contents were determined through the provided protocol of a Triglyceride Colorimetric/Fluorometric Quantification Kit (Sigma #MAK266; Zenbio #TG-1-NC).

QUANTIFICATION AND STATISTICAL ANALYSIS

Statistical significance was assessed by two-tailed Student's unpaired t-test for two-group comparisons. Two-way ANOVA followed was used for multiple group comparisons. Data are means with individual datapoints and error bars are expressed as ± SEM. $P < 0.05$ was considered significant in all the experiments. The statistical parameters and the number of mice used per experiment are found in the figure legends. Mouse experiments were performed in biological duplicate or triplicate with at least three mice per group. Cell culture experiments were collected from three or four independent cultures for each sample. The flow cytometric analysis software, FlowJo, was used to analyze cell populations and antibody staining. NIH Fiji Image J software was used to quantify co-localization, three random fields were assessed from at least three mice/cohort. The Leica Application Suite X Microscope software was used for image acquisition and analyses. All graphs and statical analysis were performed using GraphPad Prism 7–9. Excel was used for raw data collection, analysis, and quantification. Illustrations and experimental designs were created using PowerPoint and BioRender (https://www.biorender.com/)

Supplementary Material

Refer to Web version on PubMed Central for supplementary material.

ACKNOWLEDGMENTS

We would like to thank the Human Nutrition Chemistry Service Laboratory and Olga Malysheva for support and technical assistance performing liquid chromatograph mass spectrophotometry. The authors thank the Cornell Biotechnology Resources Center Flow Cytometric Core Facility and the Center of Animal Resources and Education for excellent assistance with experimental collection and mouse husbandry, respectively. This work was supported by Cornell University internal funds, and D.C.B is supported by NIH-NIDDK award R01 DK132264-01.

REFERENCES

1. Cannon B, and Nedergaard J. (2004). Brown adipose tissue: function and physiological significance. Physiol. Rev 84, 277–359. 10.1152/physrev.00015.2003. [PubMed: 14715917]
2. Cohen P, and Spiegelman BM (2015). Brown and Beige Fat: Molecular Parts of a Thermogenic Machine. Diabetes 64, 2346–2351. 10.2337/db15-0318. [PubMed: 26050670]
3. Bartelt A, and Heeren J. (2014). Adipose tissue browning and metabolic health. Nat. Rev. Endocrinol 10, 24–36. 10.1038/nrendo.2013.204. [PubMed: 24146030]
4. Nedergaard J, and Cannon B. (2014). The browning of white adipose tissue: some burning issues. Cell Metabol. 20, 396–407. 10.1016/j.cmet.2014.07.005.

5. Sidossis L, and Kajimura S. (2015). Brown and beige fat in humans: thermogenic adipocytes that control energy and glucose homeostasis. J. Clin. Invest 125, 478–486. 10.1172/JCI78362. [PubMed: 25642708]
6. Wang W, and Seale P. (2016). Control of brown and beige fat development. Nat. Rev. Mol. Cell Biol 17, 691–702. 10.1038/nrm.2016.96. [PubMed: 27552974]
7. Graja A, and Schulz TJ (2015). Mechanisms of aging-related impairment of brown adipocyte development and function. Gerontology 61, 211–217. 10.1159/000366557. [PubMed: 25531079]
8. Bartness TJ, Shrestha YB, Vaughan CH, Schwartz GJ, and Song CK (2010). Sensory and sympathetic nervous system control of white adipose tissue lipolysis. Mol. Cell. Endocrinol 318, 34–43. 10.1016/j.mce.2009.08.031. [PubMed: 19747957]
9. Zeng W, Pirzgalska RM, Pereira MMA, Kubasova N, Barateiro A, Seixas E, Lu YH, Kozlova A, Voss H, Martins GG, et al. (2015). Sympathetic neuro-adipose connections mediate leptin-driven lipolysis. Cell 163, 84–94. 10.1016/j.cell.2015.08.055. [PubMed: 26406372]
10. Bartness TJ, Vaughan CH, and Song CK (2010). Sympathetic and sensory innervation of brown adipose tissue. Int. J. Obes 34, S36–S42. 10.1038/ijo.2010.182.
11. Carmeliet P. (2003). Blood vessels and nerves: common signals, pathways and diseases. Nat. Rev. Genet 4, 710–720. 10.1038/nrg1158. [PubMed: 12951572]
12. Cui X, Jing J, Wu R, Cao Q, Li F, Li K, Wang S, Yu L, Schwartz G, Shi H, et al. (2021). Adipose tissue-derived neurotrophic factor 3 regulates sympathetic innervation and thermogenesis in adipose tissue. Nat. Commun 12, 5362. 10.1038/s41467-021-25766-2. [PubMed: 34508100]
13. Zeng X, Ye M, Resch JM, Jedrychowski MP, Hu B, Lowell BB, Ginty DD, and Spiegelman BM (2019). Innervation of thermogenic adipose tissue via a calsyntenin 3beta-S100b axis. Nature 569, 229–235. 10.1038/s41586-019-1156-9. [PubMed: 31043739]
14. Chi J, Wu Z, Choi CHJ, Nguyen L, Tegegne S, Ackerman SE, Crane A, Marchildon F, Tessier-Lavigne M, and Cohen P. (2018). Three-Dimensional Adipose Tissue Imaging Reveals Regional Variation in Beige Fat Biogenesis and PRDM16-Dependent Sympathetic Neurite Density. Cell Metabol. 27, 226–236.e3. 10.1016/j.cmet.2017.12.011.
15. Kenney MJ, and Ganta CK (2014). Autonomic nervous system and immune system interactions. Compr. Physiol 4, 1177–1200. 10.1002/cphy.c130051. [PubMed: 24944034]
16. Morrison SF (2016). Central neural control of thermoregulation and brown adipose tissue. Auton. Neurosci 196, 14–24. 10.1016/j.autneu.2016.02.010. [PubMed: 26924538]
17. Hu B, Jin C, Zeng X, Resch JM, Jedrychowski MP, Yang Z, Desai BN, Banks AS, Lowell BB, Mathis D, and Spiegelman BM (2020). gammadelta T cells and adipocyte IL-17RC control fat innervation and thermogenesis. Nature 578, 610–614. 10.1038/s41586-020-2028-z. [PubMed: 32076265]
18. Villarroya F, Cereijo R, Villarroya J, and Giralt M. (2017). Brown adipose tissue as a secretory organ. Nat. Rev. Endocrinol 13, 26–35. 10.1038/nrendo.2016.136. [PubMed: 27616452]
19. Pirzgalska RM, Seixas E, Seidman JS, Link VM, Sánchez NM,Mahú I, Mendes R, Gres V, Kubasova N, Morris I, et al. (2017). Sympathetic neuron-associated macrophages contribute to obesity by importing and metabolizing norepinephrine. Nat. Med 23, 1309–1318. 10.1038/nm.4422. [PubMed: 29035364]
20. Fischer K, Ruiz HH, Jhun K, Finan B, Oberlin DJ, van der Heide V, Kalinovich AV, Petrovic N, Wolf Y, Clemmensen C, et al. (2017). Alternatively activated macrophages do not synthesize catecholamines or contribute to adipose tissue adaptive thermogenesis. Nat. Med 23, 623–630. 10.1038/nm.4316. [PubMed: 28414329]
21. Fischer AW, de Jong JMA, Sass F, Schlein C, Heeren J, and Petrovic N. (2020). Thermoneutrality-Induced Macrophage Accumulation in Brown Adipose Tissue Does Not Impair the Tissue's Competence for Cold-Induced Thermogenic Recruitment. Front. Endocrinol 11, 568682. 10.3389/fendo.2020.568682.
22. Wolf Y, Boura-Halfon S, Cortese N, Haimon Z, Sar Shalom H, Kuperman Y, Kalchenko V, Brandis A, David E, Segal-Hayoun Y, et al. (2017). Brown-adipose-tissue macrophages control tissue innervation and homeostatic energy expenditure. Nat. Immunol 18, 665–674. 10.1038/ni.3746. [PubMed: 28459435]

23. Villarroya F, Cereijo R, Villarroya J, Gavaldà-Navarro A, and Giralt M. (2018). Toward an Understanding of How Immune Cells Control Brown and Beige Adipobiology. Cell Metabol. 27, 954–961. 10.1016/j.cmet.2018.04.006.
24. Majesky MW, Dong XR, Regan JN, and Hoglund VJ (2011). Vascular smooth muscle progenitor cells: building and repairing blood vessels. Circ. Res 108, 365–377. 10.1161/CIRCRESAHA.110.223800. [PubMed: 21293008]
25. Armulik A, Genové G, and Betsholtz C. (2011). Pericytes: developmental, physiological, and pathological perspectives, problems, and promises. Dev. Cell 21, 193–215. 10.1016/j.devcel.2011.07.001. [PubMed: 21839917]
26. Shamsi F, Piper M, Ho LL, Huang TL, Gupta A, Streets A, Lynes MD, and Tseng YH (2021). Vascular smooth muscle-derived Trpv1(+) progenitors are a source of cold-induced thermogenic adipocytes. Nat. Metab 3, 485–495. 10.1038/s42255-021-00373-z. [PubMed: 33846638]
27. Jiang Y, Berry DC, Tang W, and Graff JM (2014). Independent stem cell lineages regulate adipose organogenesis and adipose homeostasis. Cell Rep. 9, 1007–1022. 10.1016/j.celrep.2014.09.049. [PubMed: 25437556]
28. Berry DC, Jiang Y, and Graff JM (2016). Mouse strains to study cold-inducible beige progenitors and beige adipocyte formation and function. Nat. Commun 7, 10184. 10.1038/ncomms10184. [PubMed: 26729601]
29. Long JZ, Svensson KJ, Tsai L, Zeng X, Roh HC, Kong X, Rao RR, Lou J, Lokurkar I, Baur W, et al. (2014). A Smooth Muscle-Like Origin for Beige Adipocytes. Cell Metabol. 19, 810–820. 10.1016/j.cmet.2014.03.025.
30. Ivanova A, Signore M, Caro N, Greene NDE, Copp AJ, and Martinez-Barbera JP (2005). In vivo genetic ablation by Cre-mediated expression of diphtheria toxin fragment A. Genesis 43, 129–135. 10.1002/gene.20162. [PubMed: 16267821]
31. Wendling O, Bornert JM, Chambon P, and Metzger D. (2009). Efficient temporally-controlled targeted mutagenesis in smooth muscle cells of the adult mouse. Genesis 47, 14–18. 10.1002/dvg.20448. [PubMed: 18942088]
32. Soriano P. (1999). Generalized lacZ expression with the ROSA26 Cre reporter strain. Nat. Genet 21, 70–71. 10.1038/5007. [PubMed: 9916792]
33. Jiang Y, Berry DC, and Graff JM (2017). Distinct cellular and molecular mechanisms for beta3 adrenergic receptor-induced beige adipocyte formation. Elife 6, e30329. 10.7554/eLife.30329.
34. Lee S, Benvie AM, Park HG, Spektor R, Harlan B, Brenna JT, Berry DC, and Soloway PD (2022). Remodeling of gene regulatory networks underlying thermogenic stimuli-induced adipose beiging. Commun. Biol 5, 584. 10.1038/s42003-022-03531-5. [PubMed: 35701601]
35. Kim D, Kim J, Yoon JH, Ghim J, Yea K, Song P, Park S, Lee A, Hong CP, Jang MS, et al. (2014). CXCL12 secreted from adipose tissue recruits macrophages and induces insulin resistance in mice. Diabetologia 57, 1456–1465. 10.1007/s00125-014-3237-5. [PubMed: 24744121]
36. Kurita K, Ishikawa K, Takeda K, Fujimoto M, Ono H, Kumagai J, Inoue H, Yokoh H, and Yokote K. (2019). CXCL12-CXCR4 pathway activates brown adipocytes and induces insulin resistance in CXCR4-deficient mice under high-fat diet. Sci. Rep 9, 6165. 10.1038/s41598-019-42127-8. [PubMed: 30992469]
37. Ding L, and Morrison SJ (2013). Haematopoietic stem cells and early lymphoid progenitors occupy distinct bone marrow niches. Nature 495, 231–235. 10.1038/nature11885. [PubMed: 23434755]
38. Greenbaum A, Hsu YMS, Day RB, Schuettpelz LG, Christopher MJ, Borgerding JN, Nagasawa T, and Link DC (2013). CXCL12 in early mesenchymal progenitors is required for haematopoietic stem-cell maintenance. Nature 495, 227–230. 10.1038/nature11926. [PubMed: 23434756]
39. Ferreira A, and Caceres A. (1992). Expression of the class III beta-tubulin isotype in developing neurons in culture. J. Neurosci. Res 32, 516–529. 10.1002/jnr.490320407. [PubMed: 1527798]
40. Barbatelli G, Murano I, Madsen L, Hao Q, Jimenez M, Kristiansen K, Giacobino JP, De Matteis R, and Cinti S. (2010). The emergence of cold-induced brown adipocytes in mouse white fat depots is determined predominantly by white to brown adipocyte transdifferentiation. Am. J. Physiol. Endocrinol. Metab 298, E1244–E1253. 10.1152/ajpendo.00600.2009. [PubMed: 20354155]

41. Guilherme A, Yenilmez B, Bedard AH, Henriques F, Liu D, Lee A, Goldstein L, Kelly M, Nicoloro SM, Chen M, et al. (2020). Control of Adipocyte Thermogenesis and Lipogenesis through beta3-Adrenergic and Thyroid Hormone Signal Integration. Cell Rep. 31, 107598. 10.1016/j.celrep.2020.107598.
42. Lidell ME, Betz MJ, and Enerbäck S. (2014). Brown adipose tissue and its therapeutic potential. J. Intern. Med 276, 364–377. 10.1111/joim.12255. [PubMed: 24717051]
43. Nagasawa T. (2014). CXC chemokine ligand 12 (CXCL12) and its receptor CXCR4. J. Mol. Med 92, 433–439. 10.1007/s00109-014-1123-8. [PubMed: 24722947]
44. Liekens S, Schols D, and Hatse S. (2010). CXCL12-CXCR4 axis in angiogenesis, metastasis and stem cell mobilization. Curr. Pharmaceut. Des 16, 3903–3920. 10.2174/138161210794455003.
45. O'Neill LAJ, Kishton RJ, and Rathmell J. (2016). A guide to immunometabolism for immunologists. Nat. Rev. Immunol 16, 553–565. 10.1038/nri.2016.70. [PubMed: 27396447]
46. Lumeng CN, Bodzin JL, and Saltiel AR (2007). Obesity induces a phenotypic switch in adipose tissue macrophage polarization. J. Clin. Invest 117, 175–184. 10.1172/JCI29881. [PubMed: 17200717]
47. Viola A, Munari F, Sánchez-Rodríguez R, Scolaro T, and Castegna A. (2019). The Metabolic Signature of Macrophage Responses. Front. Immunol 10, 1462. 10.3389/fimmu.2019.01462. [PubMed: 31333642]
48. Ganeshan K, and Chawla A. (2017). Warming the mouse to model human diseases. Nat. Rev. Endocrinol 13, 458–465. 10.1038/nrendo.2017.48. [PubMed: 28497813]
49. Tian XY, Ganeshan K, Hong C, Nguyen KD, Qiu Y, Kim J, Tangirala RK, Tontonoz P, and Chawla A. (2016). Thermoneutral Housing Accelerates Metabolic Inflammation to Potentiate Atherosclerosis but Not Insulin Resistance. Cell Metabol. 23, 165–178. 10.1016/j.cmet.2015.10.003.
50. Chouchani ET, Kazak L, and Spiegelman BM (2019). New Advances in Adaptive Thermogenesis: UCP1 and Beyond. Cell Metabol 29, 27–37. 10.1016/j.cmet.2018.11.002.
51. Wang GX, Zhao XY, Meng ZX, Kern M, Dietrich A, Chen Z, Cozacov Z, Zhou D, Okunade AL, Su X, et al. (2014). The brown fat-enriched secreted factor Nrg4 preserves metabolic homeostasis through attenuation of hepatic lipogenesis. Nat. Med 20, 1436–1443. 10.1038/nm.3713. [PubMed: 25401691]
52. Hondares E, Iglesias R, Giralt A, Gonzalez FJ, Giralt M, Mampel T, and Villarroya F. (2011). Thermogenic activation induces FGF21 expression and release in brown adipose tissue. J. Biol. Chem 286, 12983–12990. 10.1074/jbc.M110.215889. [PubMed: 21317437]
53. Tseng YH, Kokkotou E, Schulz TJ, Huang TL, Winnay JN, Taniguchi CM, Tran TT, Suzuki R, Espinoza DO, Yamamoto Y, et al. (2008). New role of bone morphogenetic protein 7 in brown adipogenesis and energy expenditure. Nature 454, 1000–1004. 10.1038/nature07221. [PubMed: 18719589]
54. Chahrour M, and Zoghbi HY (2007). The story of Rett syndrome: from clinic to neurobiology. Neuron 56, 422–437. 10.1016/j.neuron.2007.10.001. [PubMed: 17988628]
55. Wang YN, Tang Y, He Z, Ma H, Wang L, Liu Y, Yang Q, Pan D, Zhu C, Qian S, and Tang QQ (2021). Slit3 secreted from M2-like macrophages increases sympathetic activity and thermogenesis in adipose tissue. Nat. Metab 3, 1536–1551. 10.1038/s42255-021-00482-9. [PubMed: 34782792]
56. Giri J, Das R, Nylen E, Chinnadurai R, and Galipeau J. (2020). CCL2 and CXCL12 Derived from Mesenchymal Stromal Cells Cooperatively Polarize IL-10+ Tissue Macrophages to Mitigate Gut Injury. Cell Rep. 30, 1923–1934.e4. 10.1016/j.celrep.2020.01.047. [PubMed: 32049021]
57. Karlsson M, Zhang C, Méar L, Zhong W, Digre A, Katona B, Sjöstedt E, Butler L, Odeberg J, Dusart P, et al. (2021). A single-cell type transcriptomics map of human tissues. Sci. Adv 7, eabh2169. 10.1126/sciadv.abh2169.
58. Samuelson I, and Vidal-Puig A. (2020). Studying Brown Adipose Tissue in a Human in vitro Context. Front. Endocrinol 11, 629. 10.3389/fendo.2020.00629.
59. Cypess AM (2022). Reassessing Human Adipose Tissue. N. Engl. J. Med 386, 768–779. 10.1056/NEJMra2032804. [PubMed: 35196429]

60. Xue S, Lee D, and Berry DC (2023). Thermogenic adipose tissue in energy regulation and metabolic health. Front. Endocrinol 14, 1150059. 10.3389/fendo.2023.1150059.

61. Sun W, Dong H, Balaz M, Slyper M, Drokhlyansky E, Colleluori G, Giordano A, Kovanicova Z, Stefanicka P, Balazova L, et al. (2020). snRNA-seq reveals a subpopulation of adipocytes that regulates thermogenesis. Nature 587, 98–102. 10.1038/s41586-020-2856-x. [PubMed: 33116305]

62. Emont MP, Jacobs C, Essene AL, Pant D, Tenen D, Colleluori G, Di Vincenzo A, Jørgensen AM, Dashti H, Stefek A, et al. (2022). A single-cell atlas of human and mouse white adipose tissue. Nature 603, 926–933. 10.1038/s41586-022-04518-2. [PubMed: 35296864]

63. Rao J, Djeffal Y, Chal J, Marchianò F, Wang CH, Al Tanoury Z, Gapon S, Mayeuf-Louchart A, Glass I, Sefton EM, et al. (2023). Reconstructing human brown fat developmental trajectory in vitro. Dev. Cell 58, 2359–2375.e8. 10.1016/j.devcel.2023.08.001. [PubMed: 37647896]

64. Berry DC, Jiang Y, Arpke RW, Close EL, Uchida A, Reading D, Berglund ED, Kyba M, and Graff JM (2017). Cellular Aging Contributes to Failure of Cold-Induced Beige Adipocyte Formation in Old Mice and Humans. Cell Metabol. 25, 166–181. 10.1016/j.cmet.2016.10.023.

65. Yoneshiro T, Aita S, Matsushita M, Kayahara T, Kameya T, Kawai Y, Iwanaga T, and Saito M. (2013). Recruited brown adipose tissue as an antiobesity agent in humans. J. Clin. Invest 123, 3404–3408. 10.1172/JCI67803. [PubMed: 23867622]

66. Yoneshiro T, Aita S, Matsushita M, Okamatsu-Ogura Y, Kameya T, Kawai Y, Miyagawa M, Tsujisaki M, and Saito M. (2011). Age-related decrease in cold-activated brown adipose tissue and accumulation of body fat in healthy humans. Obesity 19, 1755–1760. 10.1038/oby.2011.125. [PubMed: 21566561]

67. Harms MJ, Ishibashi J, Wang W, Lim HW, Goyama S, Sato T, Kurokawa M, Won KJ, and Seale P. (2014). Prdm16 is required for the maintenance of brown adipocyte identity and function in adult mice. Cell Metabol. 19, 593–604. 10.1016/j.cmet.2014.03.007.

68. Mina AI, LeClair RA, LeClair KB, Cohen DE, Lantier L, and Banks AS (2018). CalR: A Web-Based Analysis Tool for Indirect Calorimetry Experiments. Cell Metabol. 28, 656–666.e1. 10.1016/j.cmet.2018.06.019.

69. Jun H, Ma Y, Chen Y, Gong J, Liu S, Wang J, Knights AJ, Qiao X, Emont MP, Xu XZS, et al. (2020). Adrenergic-Independent Signaling via CHRNA2 Regulates Beige Fat Activation. Dev. Cell 54, 106–116.e5. 10.1016/j.devcel.2020.05.017. [PubMed: 32533922]

70. Liu Y, Qu Y, Cheng C, Tsai PY, Edwards K, Xue S, Pandit S, Eguchi S, Sanghera N, and Barrow JJ (2023). Nipsnap1-A regulatory factor required for long-term maintenance of non-shivering thermogenesis. Mol. Metabol 75, 101770. 10.1016/j.molmet.2023.101770.

71. Fiddler JL, Xiu Y, Blum JE, Lamarre SG, Phinney WN, Stabler SP, Brosnan ME, Brosnan JT, Thalacker-Mercer AE, and Field MS (2021). Reduced Shmt2 Expression Impairs Mitochondrial Folate Accumulation and Respiration, and Leads to Uracil Accumulation in Mouse Mitochondrial DNA. J. Nutr 151, 2882–2893. 10.1093/jn/nxab211. [PubMed: 34383924]

72. Heyden KE, Fiddler JL, Xiu Y, Malysheva OV, Handzlik MK, Phinney WN, Stiles L, Stabler SP, Metallo CM, Caudill MA, and Field MS (2023). Reduced methionine synthase expression results in uracil accumulation in mitochondrial DNA and impaired oxidative capacity. PNAS Nexus 2, pgad105. 10.1093/pnasnexus/pgad105.

73. Su F, Wang F, Zhu R, and Li H. (2009). Determination of 5-Hydroxytryptamine, Norepinephrine, Dopamine and Their Metabolites in Rat Brain Tissue by LC–ESI–MS–MS. Chromatographia 69, 207–213. 10.1365/s10337-008-0879-9.

74. Hausman DB, Park HJ, and Hausman GJ (2008). Isolation and culture of preadipocytes from rodent white adipose tissue. Methods Mol. Biol 456, 201–219. 10.1007/978-1-59745-245-8_15. [PubMed: 18516563]

75. Benvie AM, Lee D, Jiang Y, and Berry DC (2024). Platelet-derived growth factor receptor beta is required for embryonic specification and confinement of the adult white adipose lineage. iScience 27, 108682. 10.1016/j.isci.2023.108682.

76. Benvie AM, Lee D, Steiner BM, Xue S, Jiang Y, and Berry DC (2023). Age-dependent Pdgfrbeta signaling drives adipocyte progenitor dysfunction to alter the beige adipogenic niche in male mice. Nat. Commun 14, 1806. 10.1038/s41467-023-37386-z. [PubMed: 37002214]

Highlights

- Vascular smooth muscle cells support BAT homeostasis and thermogenesis
- BAT SMCs express Cxcl12 to maintain sympathetic innervation and macrophage accrual
- Loss of Cxcl12 impairs cold-induced BAT thermogenesis and energy expenditure
- Cxcl12 administration to obese mice restores the BAT thermogenic niche and function

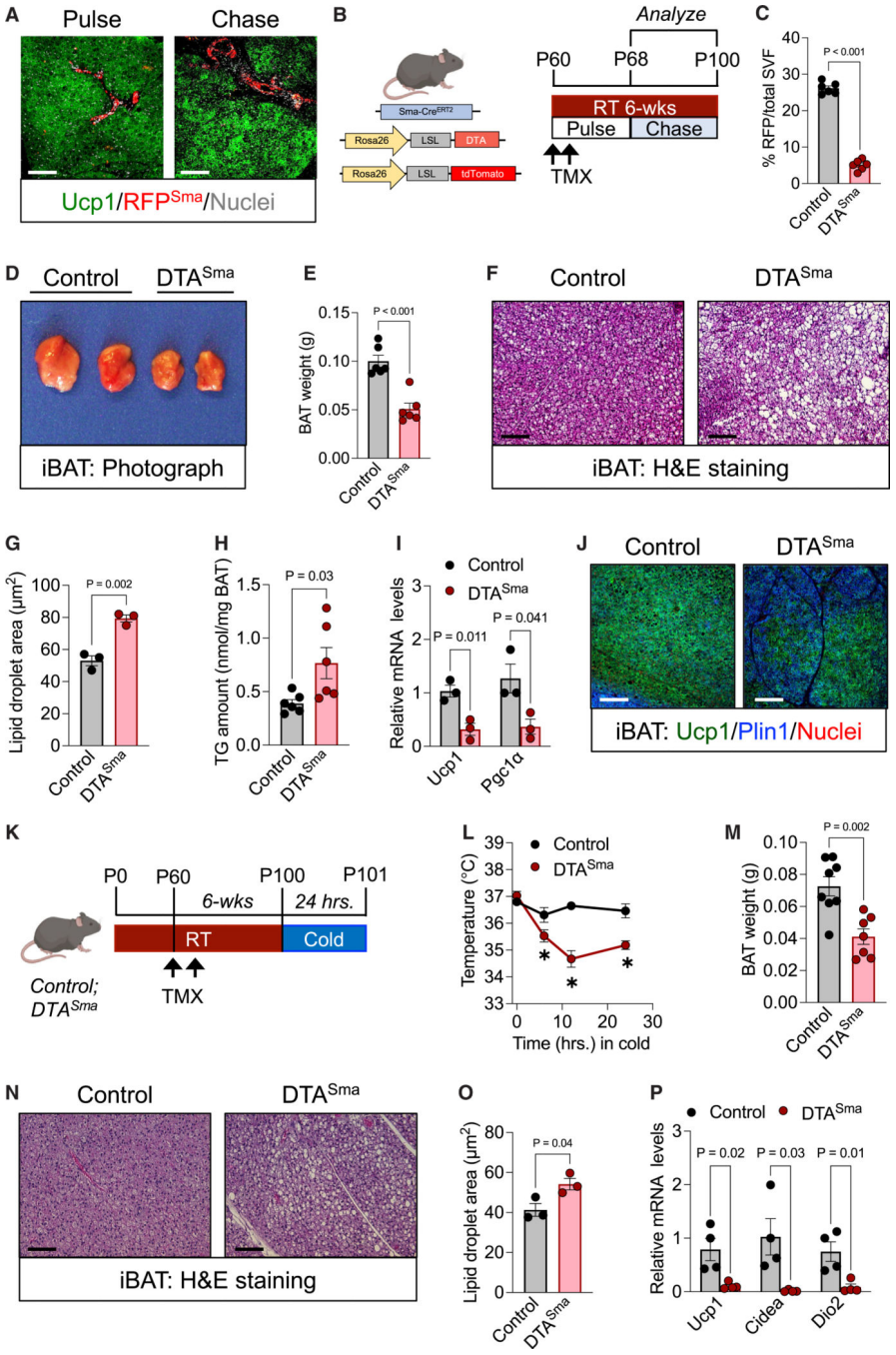

Figure 1. Vascular SMCs are critical for BAT homeostasis and function

(A) Representative images of SMC^{tdTomato} fate mapping within BAT sections from Sma-Cre^{ERT2}/Rosa26^{tdTomato} mice. Scale bars, 100 μm.

(B) Allelic combination to generate control and DTA^{Sma} mice and experimental design. Control and DTA^{Sma} mice were administered one dose of tamoxifen (50 mg/kg for 2 consecutive days and analyzed 6 weeks later.

(C) Flow cytometric analysis of BAT SMC number from mice described in (B) (n = 6 mice/group).

(D) Photograph of BAT depots from mice described in (B).
(E) BAT weight from mice described in (B) (n = 6 mice/group).
(F) Representative images of H&E staining of BAT sections from mice described in (B). Scale bars, 100 μm.
(G) Lipid droplet area quantification of images described in (F) (n = 3 mice/group).
(H) Triglyceride levels from BAT depots from mice described in (B) (n = 6 mice/group).
(I) Relative mRNA levels of thermogenic genes from mice described in (B) (n = 3 mice/group).
(J) Representative images of Ucp1 immunostaining of BAT sections from mice described in (B). Scale bars, 100 μm.
(K) Experimental design: control and DTA^{Sma} mice were administered one dose of tamoxifen for 2 consecutive days and maintained at room temperature for 6 weeks. Subsequently, the mice were exposed to cold (6.5°C) for 24 h.
(L) Intrarectal temperatures from mice described in (K) (n = 7–8 mice/group).
(M) BAT weight from mice described in (K) (n = 7–8 mice/group).
(N) Representative images of H&E staining of BAT sections from mice described in (K). Scale bars, 100 μm.
(O) Lipid droplet area quantification of images described in (N) (n = 3 mice/group).
(P) Relative mRNA levels of denoted thermogenic genes from mice described in (K) (n = 4 mice/group).
Data in (C), (E), (G–I), (L), (M), (O), and (P) are represented as the mean ± SEM. Student's unpaired t test was used to analyze denoted significance; *p < 0.03; ns, non-significant.

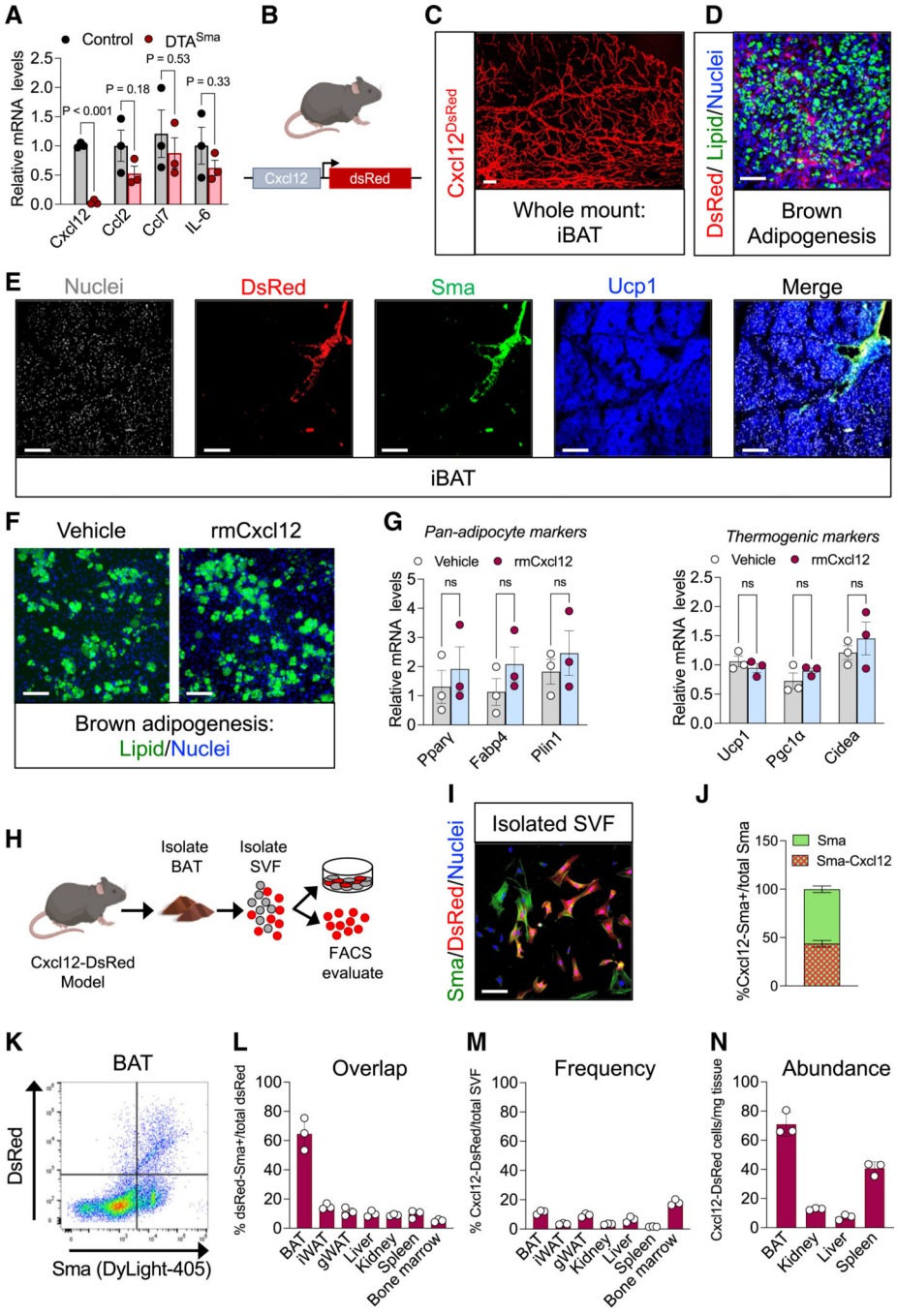

Figure 2. BAT vascular SMCs express Cxcl12

(A) Relative mRNA levels of denoted chemokine signaling pathways in BAT from control and DTA^{Sma} mice (n = 3 mice/group).

(B) Cxcl12-DsRed mouse model.

(C) Representative image of whole-mount DsRed immunofluorescent imaging of BAT from Cxcl12-DsRed mice. Scale bar, 100 μm.

(D) Representative image of *in vitro* brown adipogenesis from Cxcl12-DsRed mice. Scale bar, 100 μm.

(E) Representative images of Sma and DsRed immunostaining of BAT sections Cxcl12^{DsRed} mice. Scale bars, 100 μm.
(F) Representative images of *in vitro* brown adipogenesis treated with vehicle or recombinant murine Cxcl12 (rmCxcl12). Scale bars, 100 μm.
(G) Relative mRNA levels of denoted pan-adipocyte (left) and thermogenic (right) markers from cultures described in (F) (n = 3 mice/group).
(H) Experimental design for isolating and evaluating Cxcl12^{DsRed} cells from BAT tissues. For cell culture studies, BAT SVF cells were cultured for 24 h prior to immunostaining.
(I) Representative image of cultures described in
(H) immunostained for Sma. Scale bar, 100 μm.
(J) Quantification of Sma-Cxcl12^{DsRed} colocalization compared to total Sma^{+} cells (n = 3 mice/group).
(K) Representative fluorescence-activated cell sorting (FACS) plot identifying a Cxcl12^{DsRed}/Sma^{+} cell population within BAT.
(L) FACS analysis of Cxcl12^{DsRed}/Sma^{+} cell population compared to total DsRed cell number from denoted tissues (n = 3 mice/group).
(M) Cxcl12^{DsRed}/Sma^{+} cell population frequency from denoted tissues (n = 3 mice/group).
(N) Cxcl12^{DsRed}/Sma^{+} cell population abundance from denoted tissues (n = 3 mice/group).
Data in (A), (G), (J), and (L–N) are represented as the mean ± SEM. Student's unpaired t test was used to analyze denoted significance (ns, non-significant).

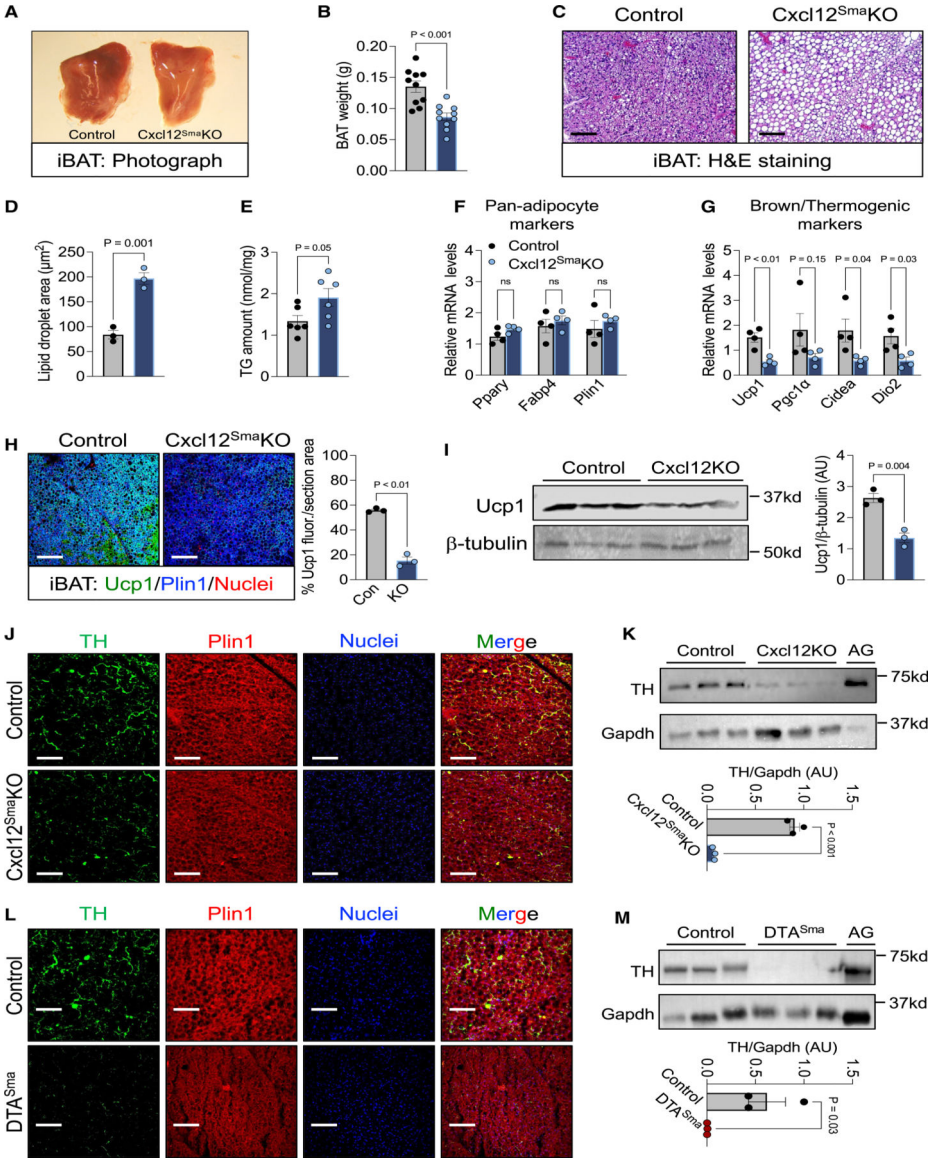

Figure 3. SMC-derived Cxcl12 expression is necessary for BAT homeostasis

(A) Representative photograph of BAT from control and Cxcl12^{Sma}KO mice 6 weeks post-tamoxifen.

(B) BAT weight from mice described in (A) (n = 10 mice/group).

(C) Representative H&E image of BAT sections from mice described in (A). Scale bars, 100 μm.

(D) Lipid droplet area quantification of images described in (C) (n = 3 mice/group).

(E) Triglyceride levels from BAT depots from mice described in (A) (n = 6 mice/group).

(F) Relative mRNA levels of pan-adipocyte markers from BAT from mice described in (A) (n = 4 mice/group).

(G) Relative mRNA levels of thermogenic genes from BAT from mice described in (A) (n = 4 mice/group).

(H) Representative images of Ucp1 immunostaining of BAT sections from mice described in (A). Scale bars, 100 μm. Right: quantification of percentage Ucp1 area in BAT sections from control and Cxcl12^{Sma}KO mice (n = 3 mice/group).
(I) Representative Ucp1 immunoblot from BAT from mice described in (A). Right: quantification of immunoblot (n = 3 mice/group).
(J) Representative images of TH immunostaining in BAT sections from mice described in (A). Scale bars, 100 μm.
(K) Representative TH immunoblot from BAT from mice described in (A). Bottom: quantification of immunoblot (n = 3 mice/group). Adrenal gland (AG) was used as a positive TH control.
(L) Representative images of TH immunostaining in BAT sections from control and DTA^{Sma} male mice 6 weeks post-tamoxifen. Scale bars, 100 μm.
(M) Representative TH immunoblot from BAT from mice described in (L). Bottom: quantification of immunoblot (n = 3 mice/group). AG was used as a positive TH control.
Data in (B), (D–I), (K), and (M) are represented as the mean ± SEM. Student's unpaired t test was used to analyze denoted significance. *$p < 0.05$; ns, non-significant.

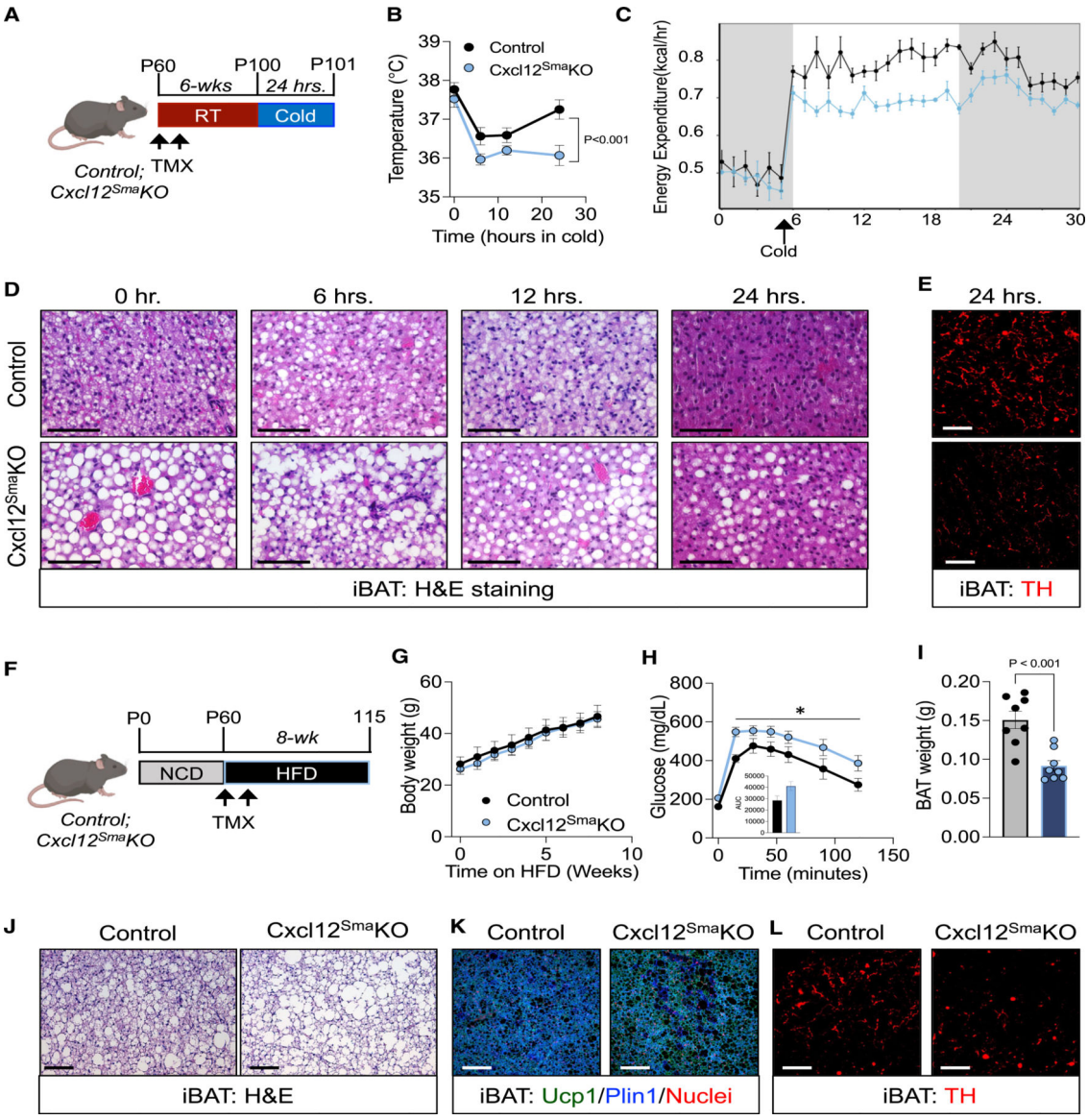

Figure 4. Loss of Cxcl12 dampens BAT thermogenesis and susceptibility to HFD BAT remodeling

(A) Experimental design: TMX-induced control and Cxcl12^{Sma}KO mice were maintained at room temperature for 6 weeks. Subsequently, mice were cold exposed (6.5°C) for 24 h.

(B) Intrarectal temperatures from mice described in (A) (n = 8 mice/group).

(C) Energy expenditure of control and Cxcl12^{Sma}KO mice maintained at room temperature (RT) and subsequently exposed to cold (n = 8 mice/group).

(D) Representative images of H&E staining of BAT sections from mice described in (A) at denoted time points throughout cold exposure. Scale bars, 100 μm.

(E) Representative images of TH immunostaining of BAT sections from mice described in (A). Scale bars, 100 μm.

(F) Experimental design: at P60, TMX-induced control and Cxcl12^{Sma}KO male mice were fed an HFD for 6 weeks and phenotypically evaluated.

(G) Body-weight curve from mice described in (F) (n = 8 mice/group).

(H) Intraperitoneal glucose tolerance test from mice described in (F). Inset: area under the curve calculation (n = 8 mice/group).
(I) BAT weight from mice described in (F) (n = 8 mice/group).
(J) Representative images of H&E staining from BAT sections from mice described in (F). Scale bars, 100 μm.
(K) Representative images of Ucp1 immunostaining of BAT sections from mice described in (F). Scale bars, 100 μm.
(L) Representative images of TH immunostaining of BAT sections from mice described in (F). Scale bars, 100 μm.
Data in (B), (C), and (G–I) are represented as the mean ± SEM. Student's unpaired t test was used to analyze denoted significance; *p < 0.03; ns, non-significant.

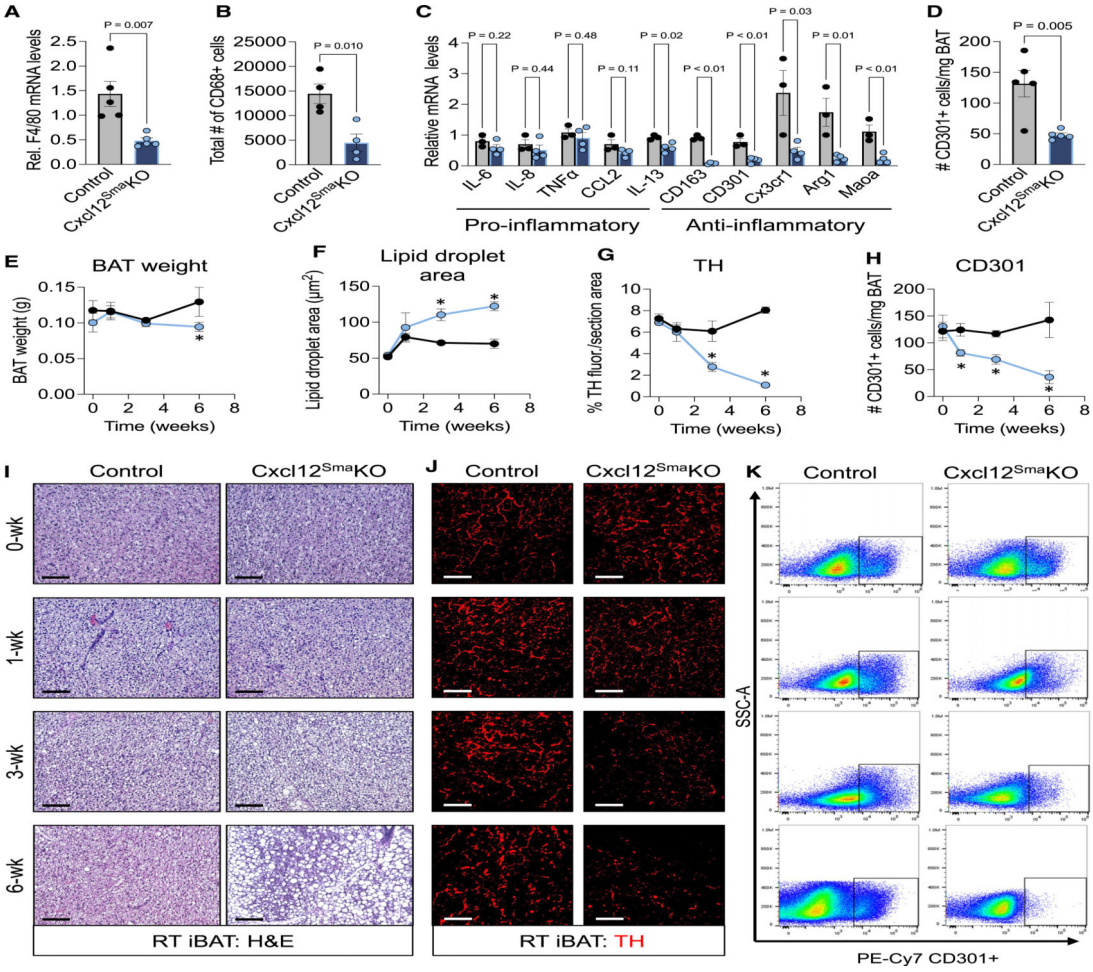

Figure 5. Cxcl12 mediates BAT macrophage accrual and sympathetic innervation

(A) Relative mRNA levels of F4/80 within BAT from control and Cxcl12^{Sma}KO mice 6 weeks post-TMX (n = 5 mice/group).

(B) Flow cytometric analysis of total CD68 cell number from BAT depots from mice described in (A) (n = 4 mice/group).

(C) Relative mRNA levels of denoted pro-inflammatory and anti-inflammatory markers from mice described in (A) (n = 3–4 mice/group).

(D) Flow cytometric analysis of CD301 abundance from BAT depots from mice described in (A) (n = 5 mice/group).

(E–K) At P60, control and Cxcl12^{Sma}KO mice were administered TMX and evaluated 0, 1, 3, and 6 week post-TMX induction. BAT weights (E), lipid drop area quantification (F), TH fluorescent area quantification (G), CD301 abundance (H), H&E staining (I), TH immunostaining (J), and CD301 flow cytometric analysis (K) were assessed. Scale bars, 100 μm.

Data in (A–H) are represented as the mean ± SEM. Student's unpaired t test was used to analyze denoted significance; *p < 0.03.

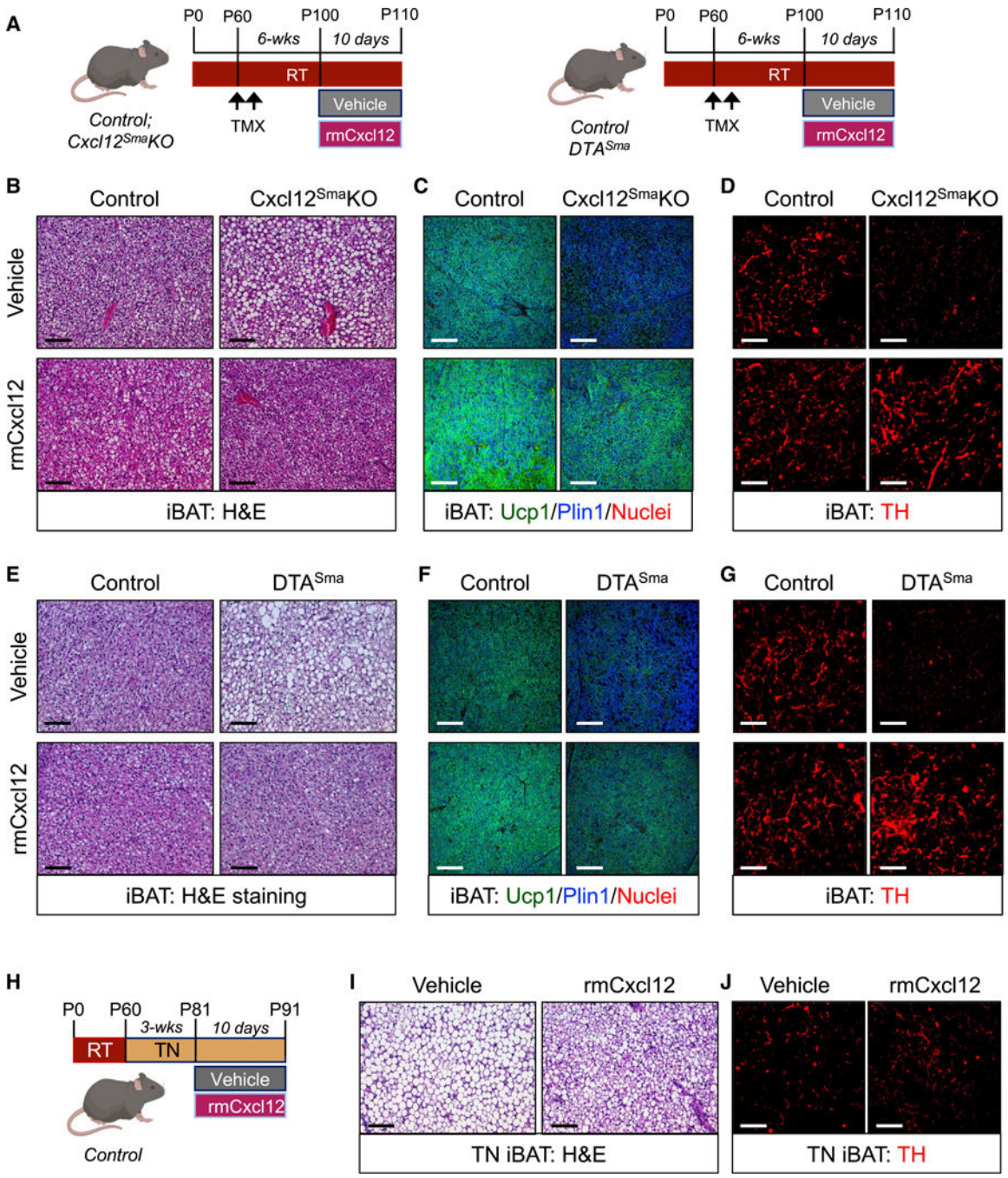

Figure 6. Exogenous Cxcl12 restores BAT homeostasis and sympathetic innervation

(A) Experimental design: at P60, Control^{Sma} and Cxcl12^{Sma}KO mice (left) or Control^{Sma} and DTA^{Sma} mice (right) were administered TMX and maintained at RT for 6 weeks. Subsequently, the mice were administered one dose of rmCxcl12 (100 ng/mouse) for 10 consecutive days.

(B) Representative H&E image of BAT sections from Control^{Sma} and Cxcl12^{Sma}KO mice described in (A). Scale bars, 100 μm.

(C) Representative images of Ucp1 immunostaining of BAT sections from Control^{Sma} and Cxcl12^{Sma}KO mice described in (A). Scale bars, 100 μm.
(D) Representative images of TH immunostaining of BAT sections from Control^{Sma} and Cxcl12^{Sma}KO mice described in (A). Scale bars, 100 μm.
(E) Representative H&E image of BAT sections from Control^{Sma} and DTA^{Sma} mice described in (A). Scale bars, 100 μm.
(F) Representative images of Ucp1 immunostaining of BAT sections from Control^{Sma} and DTA^{Sma}KO mice described in (A). Scale bars, 100 μm.
(G) Representative images of TH immunostaining of BAT sections from Control^{Sma} and DTA^{Sma}KO mice described in (A). Scale bars, 100 μm.
(H) Experimental design: at P60, RT-reared Control^{Sma} male mice were housed at thermoneutrality (30°C) for 3 weeks. Subsequently, the mice were administered one dose of rmCxcl12 (100 ng/mouse) for 10 consecutive days.
(I) Representative images of H&E staining of BAT sections from mice described in (I). Scale bars, 100 μm.
(J) Representative images of TH immunostaining of BAT sections from mice described in (I). Scale bars, 100 μm.

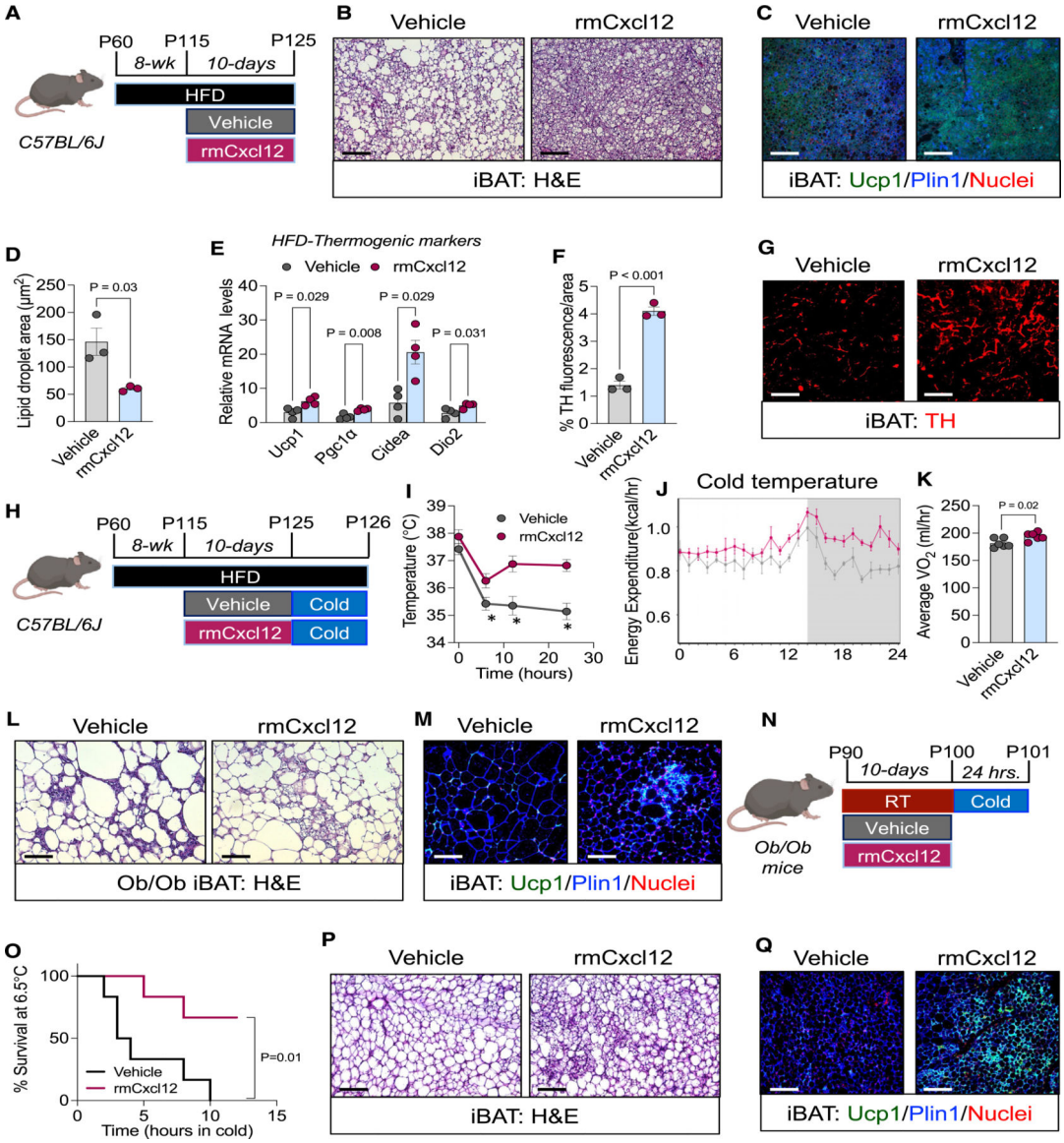

Figure 7. Exogenous Cxcl12 restores BAT function in obesogenic models

(A) Experimental design: at P60, C57BL/6J mice were fed an HFD for 8 weeks. Subsequently, the mice were administered one dose of vehicle or rmCxcl12 (100 ng/mouse) for 10 consecutive days (n = 8 mice/group).

(B) Representative images of H&E staining of BAT sections from mice described in (A). Scale bars, 100 μm.

(C) Representative images of Ucp1 immunostaining of BAT sections from mice described in (A). Scale bars, 100 μm.

(D) Lipid droplet area quantification of BAT H&E sections from mice described in (A) (n = 3 mice/group).

(E) Relative mRNA levels of denoted thermogenic genes from mice described in (A) (n = 4 mice/group).

(F) TH quantification from images described in (G) from mice described in (A) ($n = 3$ mice/group).
(G) Representative images of TH immunostaining of BAT sections from mice described in (A). Scale bars, 100 μm.
(H) Experimental design: at P60, C57BL/6J mice were fed an HFD for 8 weeks. Subsequently, the mice were administered one dose of vehicle or rmCxcl12 (100 ng/mouse) for 10 consecutive days and then exposed to cold for 24 h.
(I) Intrarectal temperatures of mice described in (H) ($n = 8$ mice/group).
(J) Energy expenditure of cold-exposed mice described (H) ($n = 6$ mice/group).
(K) Oxygen consumption of cold-exposed mice described in (H) ($n = 6$ mice/group).
(L) Representative images of H&E staining of BAT sections from mice described in (J). Scale bars, 100 μm.
(M) Representative images of Ucp1 immunostaining of BAT sections from mice described in (J). Scale bars, 100 μm.
(N) Experimental design: at P90, Ob/Ob mice were administered one dose of vehicle or rmCxcl12 (100 ng/mouse) for 10 consecutive days and subsequently exposed to cold.
(O) Survival plot of Ob/Ob male mice that received vehicle or rmCxcl12 with a surviving rectal temperature of ≥27°C ($n = 6$ mice/group).
(P) Representative images of H&E staining of BAT sections from mice described in (M). Scale bars, 100 μm.
(Q) Representative images of Ucp1 immunostaining of BAT sections from mice described in (M). Scale bars, 100 μm.
Data in (D–F), (I–K), and (O) are represented as the mean ± SEM. Student's unpaired t test was used to test significance between vehicle- and rmCxcl12-treated samples, or log-rank (Mantel-Cox) test was used to test cold-temperature-survival significance; $*p < 0.01$.

KEY RESOURCES TABLE

REAGENT or RESOURCE	SOURCE	IDENTIFIER
Antibodies		
Alexa Fluor 568 donkey anti-rabbit IgG (H+L)	invitrogen	Cat#A10042; RRID:AB_2534017
Anti-Tyrosine Hydroxylase	EMD Millipore	Cat#AB152; RRID:AB_390204
Anti-α-Smooth Muscle Actin antibody (Clone 1A4)	R&D Systems	Cat#MAB1420; RRID:AB_262054
Anti-perilipin-1 antibody	abcam	Cat#ab61682; RRID:AB_944751
Anti-UCP-1 antibody	abcam	Cat#ab10983; RRID:AB_2241462
Alexa Fluor 647 donkey anti-goat IgG (H+L)	invitrogen	Cat#A21447; RRID:AB_2535864
Anti-Caveolin-1 Antibody (7C8)	novusbio	Cat#NB100-615; RRID:AB_10003431
Anti-mouse CD45 antibody	Biolegend	Cat#103151; RRID:AB_2565884
Anti-mouse CD301 antibody	Biolegend	Cat#145705; RRID:AB_2562939
Anti-mouse CD68 antibody	Biolegend	Cat#137003; RRID:AB_2044001
Anti-Beta-Tubulin	Cell Siganling	Cat#2146; RRID:AB_2210545
Anti-GAPDH (14C10)	Cell Signaling	Cat#2118S; RRID:AB_561053
Cy5-Donkey Anti-Mouse IgG	Jackson Immunoresearch	Cat#715-175-150; RRID:AB_2340819
Donkey anti-rabbit IgG (H+L) Cross-Adsorbed Secondary Antibody, HRP	invitrogen	Cat#31458; RRID:AB_228213
Chemicals, peptides, and recombinant proteins		
TRIzol Reagent	ambion	Cat#15596018
Phosphate buffered saline powder, pH 7.4	Sigma-Aldrich	Cat#1003015902
10% Buffered Formalin Phosphate	Fisherchemical	Cat#SF100-4
Gill 2 Hematoxlyin	Epredia	Cat#72511
Bluing Reagent	ThermoScientific	Cat#7301
High Def	StatLab	Cat#SL103
Eosin-Y	ThermoScientific	Cat#71225
Xylene Substitute	Epredia	Cat#9990505
R-Buffer A, 10X, pH 6	Electron Microscopy Sciences	Cat#62706-10
Triton X-100, 10% solution, peroxide-free	amresco	Cat#M236-10ML
Sudan Black B	Sigma-Aldrich	Cat#199664-25G
Recombinant murine CXCL12	PeproTech	Cat#250-20A
Tamoxifen	Cayman Chemical	Cat#13258
Cl316,243	Cayman Chemical	Cat#17499
DMEM/F12(1:1)(1x)	gibco	Cat#11320-033
Pen Strep	gibco	Cat#15140-122
TRIS-Tricine-SDS Running Buffer (10X)	Bio Rad	Cat#1610744
10X Tris/Glycine Buffer	Bio Rad	Cat#1610771
Precision Plus Protein Dual Color Standards	Bio Rad	Cat#1610374
HCS LipidTOX™ Green neutral lipid stain	invitrogen	Cat#H34475
Oligomycin	thermoscientific	Cat#J61898.MA

REAGENT or RESOURCE	SOURCE	IDENTIFIER
Norepinephrine	Sigma	Cat#A7257
Norepinephrine-2,5,6,α,β,β-D6	CDN Isotopes	Cat#D-6634
Critical commercial assays		
Triglyceride Quantification Coloremetric/Fluorometric Kit	Sigma-Aldrich	Cat#MAK266
High Capacity cDNA Reverse Transcription Kit	applied biosystems	Cat#4368813
Pierce BCA Protein Assay Kit	thermoscientific	Cat#23225
PowerUp SYBR Green Master Mix	appliedbiosystems	Cat#A25742
SuperSignal™ West Pico PLUS Chemiluminescent Substrate	proteinbiology	Cat#34580
Quantikine ELISA Mouse CXCL12/SDF-1α	R&D Systems	Cat#MCX120
Agilent Seahorse XFe24 Extracellular Flux Assay Kit	Agilent	N/A
Agilent Seahorse XF Calibrant (pH 7.4)	Agilent	Cat#100840-000
Experimental models: Organisms/strains		
Mouse: Cxcl12-DsRed: *Cxcl12*$^{tm2.1Sjm}$/J	The Jackson Laboratory	JAX 022458; RRID:IMSR_JAX:022458
Mouse: Cxcl12$^{fl/fl}$: B6(FVB)-*Cxcl12*$^{tm1.1Link}$/J	The Jackson Laboratory	JAX 021773; RRID:IMSR_JAX:021773
Mouse: *Ob/Ob*: B6.Cg-*Lep*^{ob}/J	The Jackson Laboratory	JAX 000632; RRID:IMSR_JAX:000632
Mouse:PPARγ^{loxP}: B6.129-*Pparγ*^{tm2Rev}/J	The Jackson Laboratory	JAX 004584; RRID:IMSR_JAX:004584
Mouse: Rosa-DTA: B6.129P2-*Gt (ROSA)26Sor*$^{tm1(DTA)Lky}$/J	The Jackson Laboratory	JAX 009669; RRID: IMSR_JAX:009669
Mouse: R26$^{-tdtomato}$: B6.Cg-*Gt* (ROSA)26Sor$^{tm14(CAG-tdTomato)Hze}$/J	The Jackson Laboratory	JAX: 007914; RRID:IMSR_JAX:007914
Mouse: Sma-Cre-ER^{T2}	Wendling et al.[31]	N/A
Mouse: C57BL/6J	The Jackson Laboratory	Strain #:000664; RRID:IMSR_JAX:000664
Software and algorithms		
Attune Cytometric Software	invitrogen	Version 5.3.2415.0
BD FACSDiva Software	BD Biosciences	Version 9.4; RRID:SCR_001456
Fiji - ImageJ Software	ImageJ2	https://ImageJ.net/; RRID:SCR_003070
FlowJo Software	FlowJo, LLC	Version 10; RRID:SCR_008520
BioRender	BioRender	http://biorender.com/; RRID:SCR_018361
Xcailbur Software	Thermo	Cat#OPTON-30965